CM² MAGAZINE

第 67 期

南方科技大学海洋磁学中心主编

https://cm2.sustech.edu.cn/

创刊词

海洋是生命的摇篮，是文明的纽带。地球上最早的生命诞生于海洋，海洋里的生命最终进化成了人类，人类的文化融合又通过海洋得以实现。人因海而兴。

人类对海洋的探索从未停止。从远古时代美丽的神话传说，到麦哲伦的全球航行，再到现代对大洋的科学钻探计划，海洋逐渐从人类敬畏崇拜幻想的精神寄托演变成可以开发利用与科学研究的客观存在。其中，上个世纪与太空探索同步发展的大洋科学钻探计划将人类对海洋的认知推向了崭新的纬度：深海（deep sea）与深时（deep time）。大洋钻探计划让人类知道，奔流不息的大海之下，埋藏的却是亿万年的地球历史。它们记录了地球板块的运动，从而使板块构造学说得到证实；它们记录了地球环境的演变，从而让古海洋学方兴未艾。

在探索海洋的悠久历史中，从大航海时代的导航，到大洋钻探计划中不可或缺的磁性地层学，磁学发挥了不可替代的作用。这不是偶然，因为从微观到宏观，磁性是最基本的物理属性之一，可以说，万物皆有磁性。基于课题组的学科背景和对海洋的理解，我们对海洋的探索以磁学为主要手段，海洋磁学中心因此而生。

海洋磁学中心，简称 CM^2，一为其全名“Centre for Marine Magnetism”的缩写，另者恰与爱因斯坦著名的质能方程 $E = MC^2$ 对称，借以表达我们对科学巨匠的敬仰和对科学的不懈追求。

然而科学从来不是单打独斗的产物。我们以磁学为研究海洋的主攻利器，但绝不仅限于磁学。凡与磁学相关的领域均是我们关注的重点。为了跟踪反映国内外地球科学特别是与磁学有关的地球科学领域的最新研究进展，海洋磁学中心特地主办 CM^2 Magazine，以期与各位地球科学工作者相互交流学习、合作共进！

“海洋孕育了生命，联通了世界，促进了发展”。21 世纪是海洋科学的时代，由陆向海，让我们携手迈进中国海洋科学的黄金时代。

目 录

一、研究进展

1. 印度-亚洲大碰撞起始于赤道湿润带

印度-亚洲大陆的初始碰撞是十分重要的科学命题。一方面初始碰撞位置和时间是建立青藏高原动力学演化模型最重要的边界条件；另一方面，初始碰撞可通过改变风化、剥蚀速率、大洋化学成分以及岩浆作用的强度对全球气候产生重要影响。因此，确定印度-亚洲大陆的初始碰撞位置和时间，是理解亚洲乃至全球构造/气候演化过程的一把钥匙。印度-亚洲大陆的初始碰撞无疑又是一个充满争议的命题。古地磁学家提出的碰撞时间从 ~65-25 Ma 不等，尽管目前大部分证据都已经指向较早的碰撞时间，即 ~65-50 Ma，但仍存在大量不能协调的问题。从古地磁的角度来讲，求解印度-亚洲初始碰撞的位置和时间理论上并不复杂，只需将印度-特提斯喜马拉雅-拉萨三个块体之间的运动学参数进行对比即可。在碰撞时间、位置这个二元命题中，后者被认为是一个更简单的问题，只要得到拉萨地块碰撞前后的古纬度即可。

然而现实的情况是，古地磁学家从林子宗群火山岩（～64-44 Ma）得到的古纬度竟然从～7°N 到～30°N 不等。虽然后续工作排除了一些来自帕那组 1 段的异常高倾角数据，但从林子宗群典中组得到的古纬度（～7°N）仍然比上部地层低 ～10°左右，并且同样也低于早白垩世 ～20°N 左右的古纬度。因此，在后续的古地磁资料分析中，典中组的数据一般被当成异常数据来处理。为进一步查明这一差异性的来源，Huang 等 (2015, Tectonic) 对林周盆地典中组的火山岩开展了进一步的古地磁研究。通过岩石磁学、岩相学以及年代学的研究，特别是岩石薄片中广泛出现的赤铁矿以及一个更年轻的 ^{40}Ar/^{39}Ar 年代学数据 （~50 Ma），提出典中组的火山岩很可能遭受了造山带流体引起的热/化学重磁化，并进一步认为重磁化的纬度为 ～20°N。这一研究似乎可以很好地协调林子宗群火山岩的古纬度差异，进一步支持初始碰撞的发生在 ～20°N。自此，印度-亚洲初始碰撞发生在 ～20°N 被广泛引用。

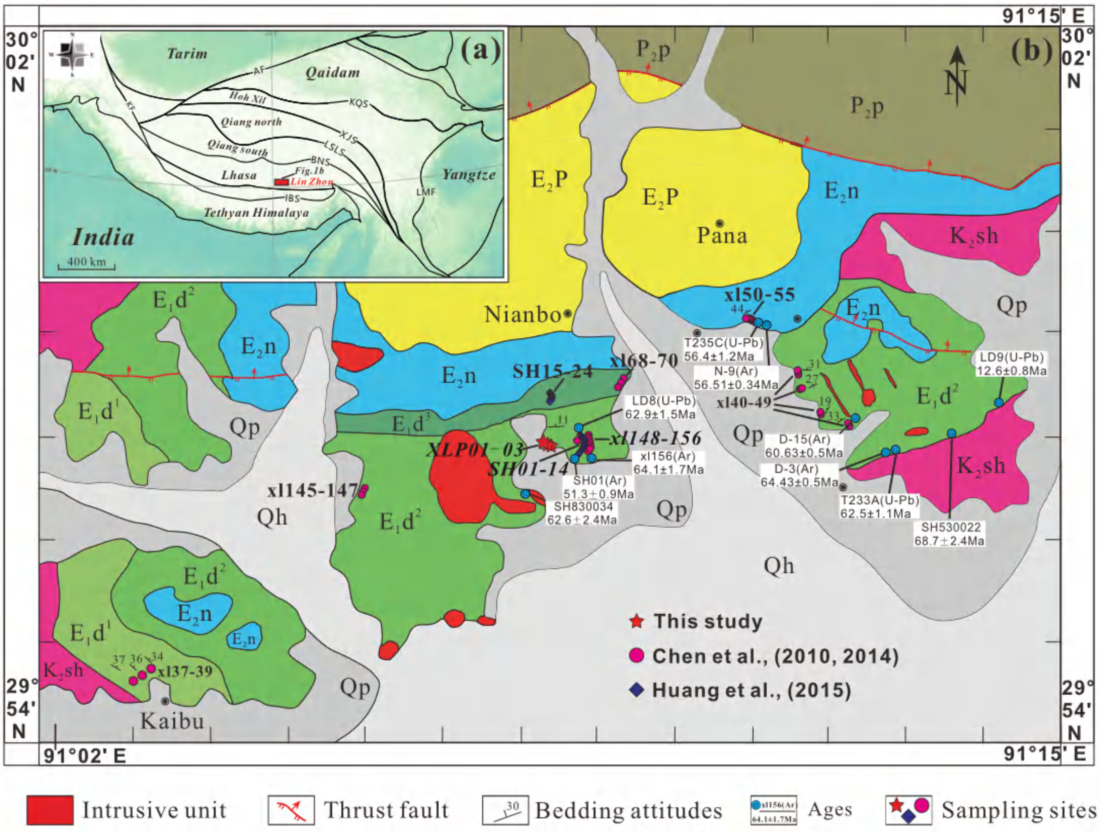

图 1. 林周盆地古地磁及年代学采样点示意图。

然而，疑点难免仍然存在。比如，典中组绝大部分同位素年龄为 ~69-58 Ma，并且 U-Pb 年龄与 40Ar/39Ar 年龄基本重合，似乎并不支持典中组出现过广泛的热重磁化；另一方面，典中组火山岩赤铁矿含量较高的层位仅限于典中三段，而前人的古地磁数据主要来自典中二段（图 1），岩石磁学和退磁结果都表明这一段主要是磁铁矿载磁，加之即便赤铁矿出现也并不能作为重磁化的标志，现有证据似乎也不支持出现过广泛的化学重磁化。显然，典中组是否遭受重磁化显然还需要进一步更严格的证明。

为进一步确定拉萨地块碰撞前的古地理位置，我们对林周盆地林子宗群典中组火山岩进行了砾石检验。在本研究中，我们从典中组二段的熔岩流夹层中找到一层约 30 米厚的火山角砾并采集 25 个岩芯样本。通过系统热退磁分析，全部样品分离得到稳定的特征剩磁。火山角砾的特征剩磁方向呈离散分布，并在 95%置信水平下通过了砾石检验。同时我们从火山角砾的上覆和下伏熔岩流中获得两个采点的特征剩磁，其方向为集中分布并且与前人获得的特征剩磁方向一致(图 2)。结合典中组详细的同位素年代学数据和载磁矿物特征，我们认为林周盆地典中组

火山岩所记录的特征剩磁为原生。同时，我们将 Chen 等 (2014, JAES), Huang 等 (2015, Tectonics) 以及本研究从熔岩流获得的特征剩磁采点平均方向进行统一分析，获得矫正后的平均方向为 D = 187.0°, I = -12.8°,□□95 = 5.4° , N=35 (图 2)。该古地磁极通过了全部可靠性判据（R=7），限定拉萨地体在 ~64-60 Ma 时的古纬度为 6.7 ± 4.4°N (图 3)。同时考虑到典中组喷发的时段（~64-60 Ma）很可能是初始碰撞的关键时期，我们认为典中组的古地磁结果为印度-亚洲初始碰撞位置提供了最直接、最可靠的约束。

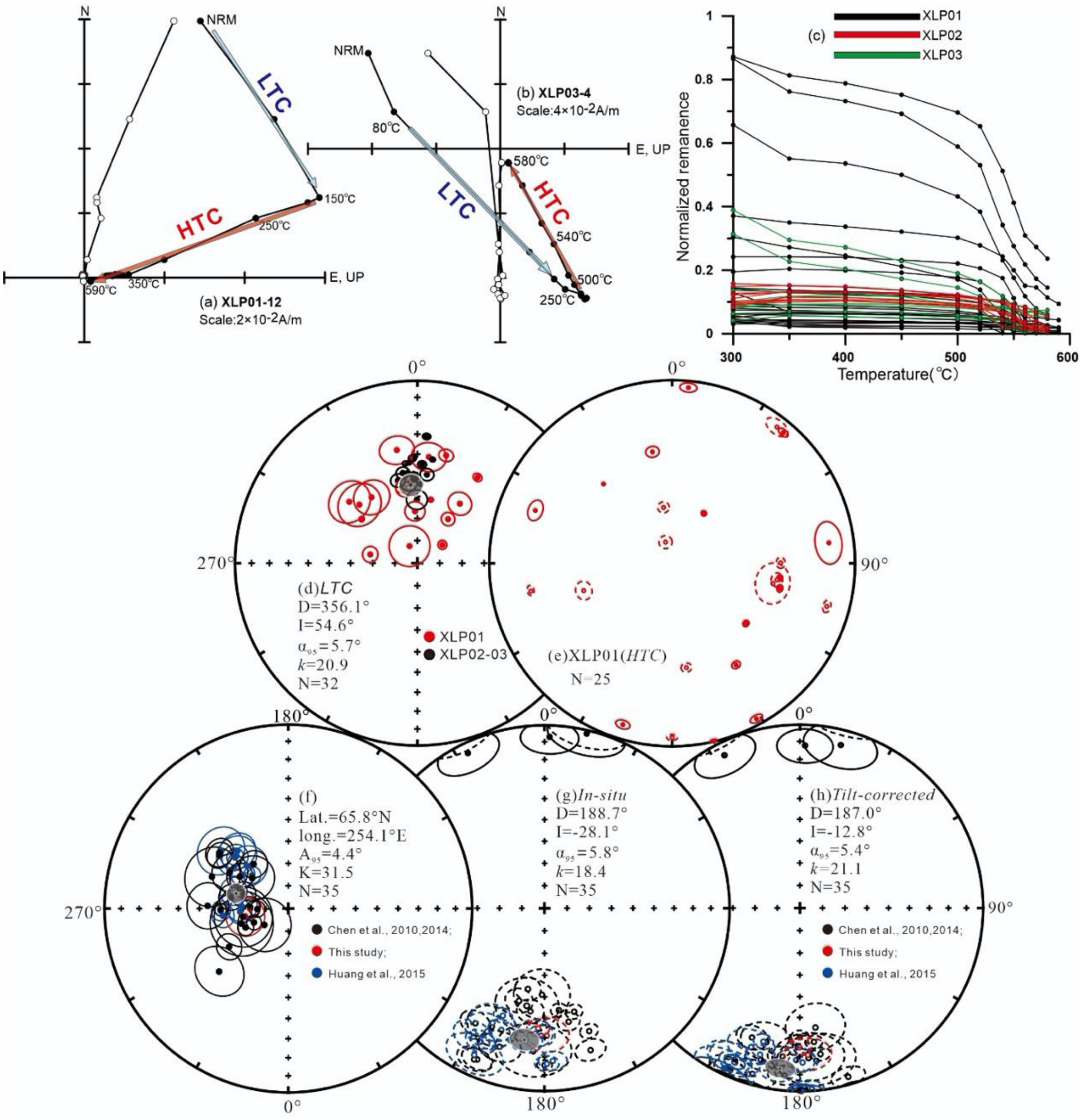

图 2. 典中组退磁曲线 (a-c)、砾石检验结果 (d, e)、虚地磁极 (f) 及特征剩磁统计 (g, h)。

然而，与林子宗群上部以及拉萨地块下白垩统古地磁结果相比，典中组的古纬度确实存在~10° 左右的偏低，如何解释这一差别是不可回避的问题。直接从

数据层面上解释，意味着拉萨地块在晚白垩世以来发生了约 1000km 左右的南向移动，继而在新生代向北漂移，才达到现今的位置。考虑到拉萨地块在早白垩世就已经与亚洲大陆完成拼合，显然这一运动不可能是拉萨地块独立完成的，而这似乎又与主流的全球视极移曲线所预测的欧亚大陆的整体运动是矛盾的。然而，亚洲大陆白垩纪以来的视极移曲线同样存在长期的争论，比如 Cogné等 (2013) 就认为欧亚大陆不是刚性的，在 ~50Ma 时亚洲大陆处于更靠南的位置（大约偏南 10°），这无疑需要亚洲大陆在晚白垩期间发生一定程度的南向移动。此外，最近天山托云盆地的古地磁研究也指示早白垩-始新世期间磁倾角发生显著降低，这也与我们计算的拉萨地块南向运动的幅度相当。基于以上考虑，我们初步认为拉萨地块晚白垩世的南向运动很可能是真实的，拉萨地块典中组与早白垩及始新世古地磁结果的差异也是客观存在的。

我们的结果表明印度-亚洲初始碰撞过程中的陆-陆、弧-陆碰撞均发生在赤道湿润带以内(图 3)，这一低纬度的初始碰撞过程可能大大加剧了硅酸盐，特别是来自大洋岛弧的基性、超基性岩的风化作用，导致额外的二氧化碳消耗，这可能是驱动新生代全球变冷的关键因素之一。这些认识对于理解印度-亚洲碰撞的构造和气候意义是至关重要的。

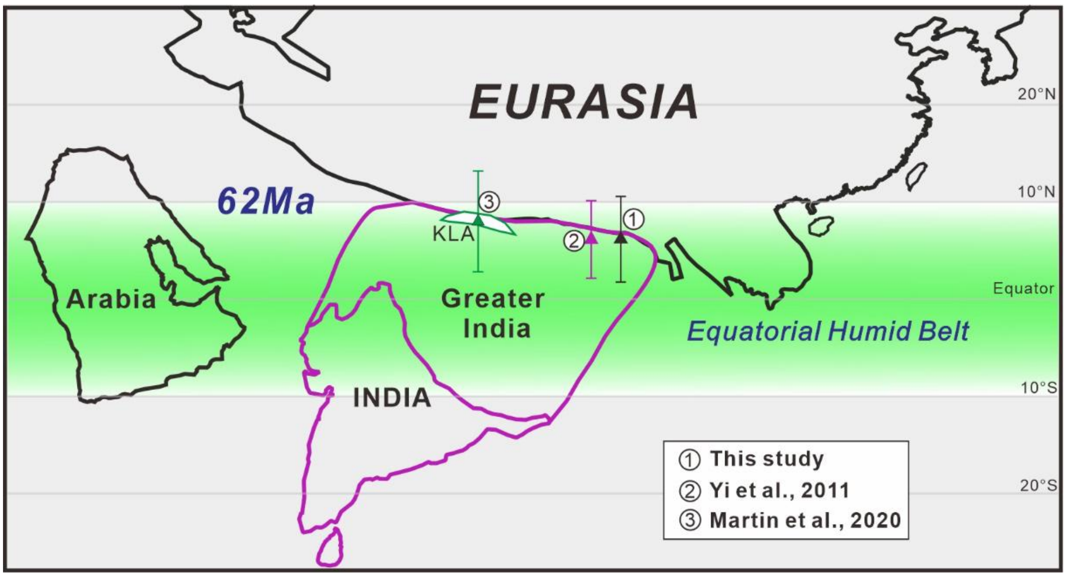

图 3. 印度-亚洲初始碰撞重建图。

该成果发表于 Geophysical Research Letters，研究得到国家自然科学基金项目 (92055205, 41672223)和中山大学百人计划启动经费(74110-18841244)资助。

Yi, Z., Wang, T., Meert, J. G., Zhao, Q., and Liu, Y. (2021). ***An initial collision of India and Asia in the equatorial humid belt****. Geophysical Research Letters, 48, e2021GL093408. https://doi.org/10.1029/2021GL093408*。

作者简介：易治宇：中山大学大气科学学院。主要研究方向：古板块/环境重建、构造/气候耦合演化。

二、文献速递

1. 晚中新世以来亚洲季风演化与太平洋温度梯度密切相关

翻译人：仲义 zhongy@sustech.edu.cn

Lu J, Yang H, Griffiths M L, et al. ***Asian monsoon evolution linked to Pacific temperature gradients since the Late Miocene[J].*** *Earth and Planetary Science Letters, 2021, 563: 116882.*https://doi.org/10.1016/j.epsl.2021.116882

摘要: 晚中新世以来对于东亚季风演化的性质和成因存在不确定性，该时期是一个明显变暖的气候时期，其特征是经向和纬向太平洋海表温度（SST）梯度比今天更弱，因此被认为是我们预测未来气候变暖趋势的潜在参考研究对象。然而，这些温度梯度在多大程度上影响了整个东亚地区的降雨模式，特别是季风区域的北部范围仍然存在争议。作者以华北平原陆相沉积层序中保存的有机生物标志物为载体，首次报道了 8 百万年以来水汽记录。记录显示在早上新世（~4.2-4.5 Ma）时期存在明显季风降水的升高，对应太平洋径向和区域性 SST 梯度以及东太平洋冷舌的增强作用。中国北方地区明显季风降水现象在亚洲南部记录中同样出现，但与中国中东部（包括华南地区）存在反相位关系，表明东亚地区呈现“三极”降水模式。通过一系列的气候模型实验，结果显示在早上新世（5.33-3.6 Ma）东亚地区季风降水重新分配主要是由于西太平洋暖池地区赤道方向的收缩，导致亚热带太平洋地区夏季对流减弱，哈德利和沃克环流作用增强。研究进一步强调了太平洋温度梯度对东亚降水起着非常重要的影响。

ABSTRACT: Considerable uncertainty remains over the nature and causes(s) of East Asian monsoon evolution since the Late Miocene, a significantly warmer period characterized by substantially weaker meridional and zonal Pacific sea surface temperature (SST) gradients than today and therefore regarded as a potential analog for current and future global warming. However, the extent to which these temperature gradients impacted rainfall patterns across East Asia, and particularly the northern

extent of the monsoon domain, remains controversial. Here we present the first hydrological record extending back eight million years (Ma) for North China Plain derived from organic biomarkers preserved in a terrestrial sediment sequence. Our record shows a significant increase in monsoon rainfall during the Early Pliocene (~4.2-4.5 Ma), coincident with strengthening of Pacific meridional and zonal SST gradients, and the eastern equatorial Pacific cold tongue. This marked intensification of the monsoon rainfall in northern China is also observed in paleoclimate archives from southern Asia, but anti-phased with those from central-eastern China (including southern China), indicating a ‘tripole-like’ rainfall pattern over East Asia. Through a set of climate model experiments, we show that this redistribution of monsoon rainfall across East Asia during the Early Pliocene (5.33-3.6 Ma) was likely due to an equatorward contraction of the western Pacific warm pool, reduced summer convection in the western subtropical Pacific, and the strengthening of the Hadley and Walker circulations. Our study thus highlights the strong influence of Pacific Ocean temperature gradients on East Asian hydroclimate.

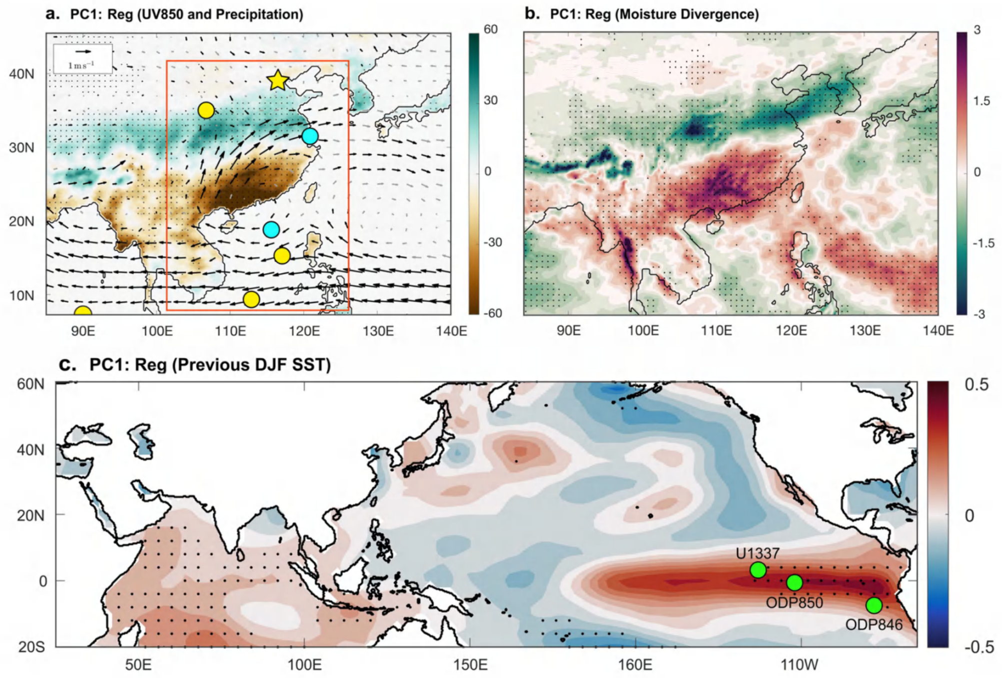

Fig1. Influence of ENSO on modern East Asian summer monsoon variability. a-b. Regression maps of East Asian July-August a, precipitation (mm, shading; PERSIANN-CDR: Ashouri et al., 2015)

and 850-hPa winds (m s-1, vectors; ECMWF ERA5), and b, vertically integrated moisture divergence (kg m-2; ECMWF ERA5) onto Principal Component 1 (PC1) of precipitation. PC1 was generated from an EOF analysis of precipitation for East Asia [red box in a (100-124◦ E, 8-45◦ N); Fig. S1]. Symbols in a indicate our study site (star), along with other records from the Chinese Loess Plateau (Sun et al., 2006), Yangtze River Delta(Zhang et al., 2013), northern South China Sea (Wan et al., 2007), central (Gai et al., 2020) and southwestern (Zhang et al., 2009) South China Sea, Bay of Bengal (An et al., 2001) (circles). Blue sites indicates wetter Pliocene conditions and yellow sites indicate drier Pliocene conditions as plotted in Fig. 5. c, Regression map of previous DJF SSTs onto PC1. Green circles indicate site locations for the cold tongue SST records mentioned in the text and shown in Fig. 6. The black vectors and black stippled regions in a-c denote significance at the 90% confidence level. (For interpretation of the colors in the figure(s), the reader is referred to the web version of this article.)

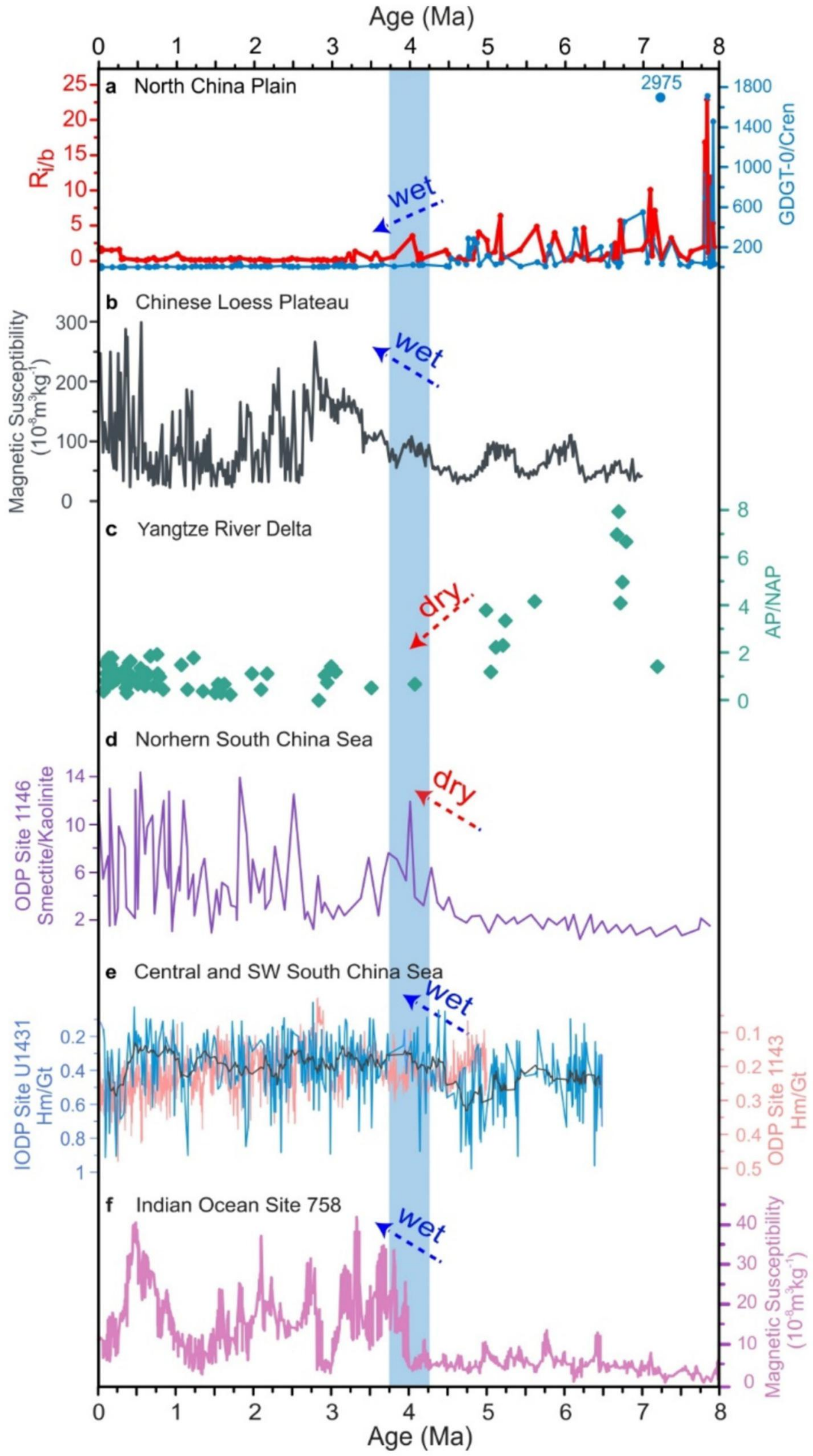

Fig2. Hydroclimate tripole pattern across East Asia during the Miocene-Pliocene. a, Ratio of GDGT-0/Cren and Ri/b proxy in the G3 core from the North China Plain. b, Loess magnetic susceptibility

data from Chinese Loess Plateau (Sun et al., 2006). c, Ratio of arboreal pollen (AP) to non arboreal pollen (NAP) of fluvial-lacustrine core ZK004 in Yangtze River Delta (Zhang et al., 2013). d, Smectite/Kaolinite records at ODP Site 1146, northern SCS (Wan et al., 2007). e, Hematite/goethite (Hm/Gt) values at IODP Site U1431, central SCS (salmon curve) (Gai et al., 2020) and ODP Site 1143, southwestern SCS (blue curve) (Zhang et al., 2009). f, Magnetic susceptibility flux from the Indian Ocean ODP Site 758 (An et al., 2001). Blue vertical bar indicates the significant hydrological changes observed across East Asia at 4.2-4.5 Ma. The black line in e is smoothed curve

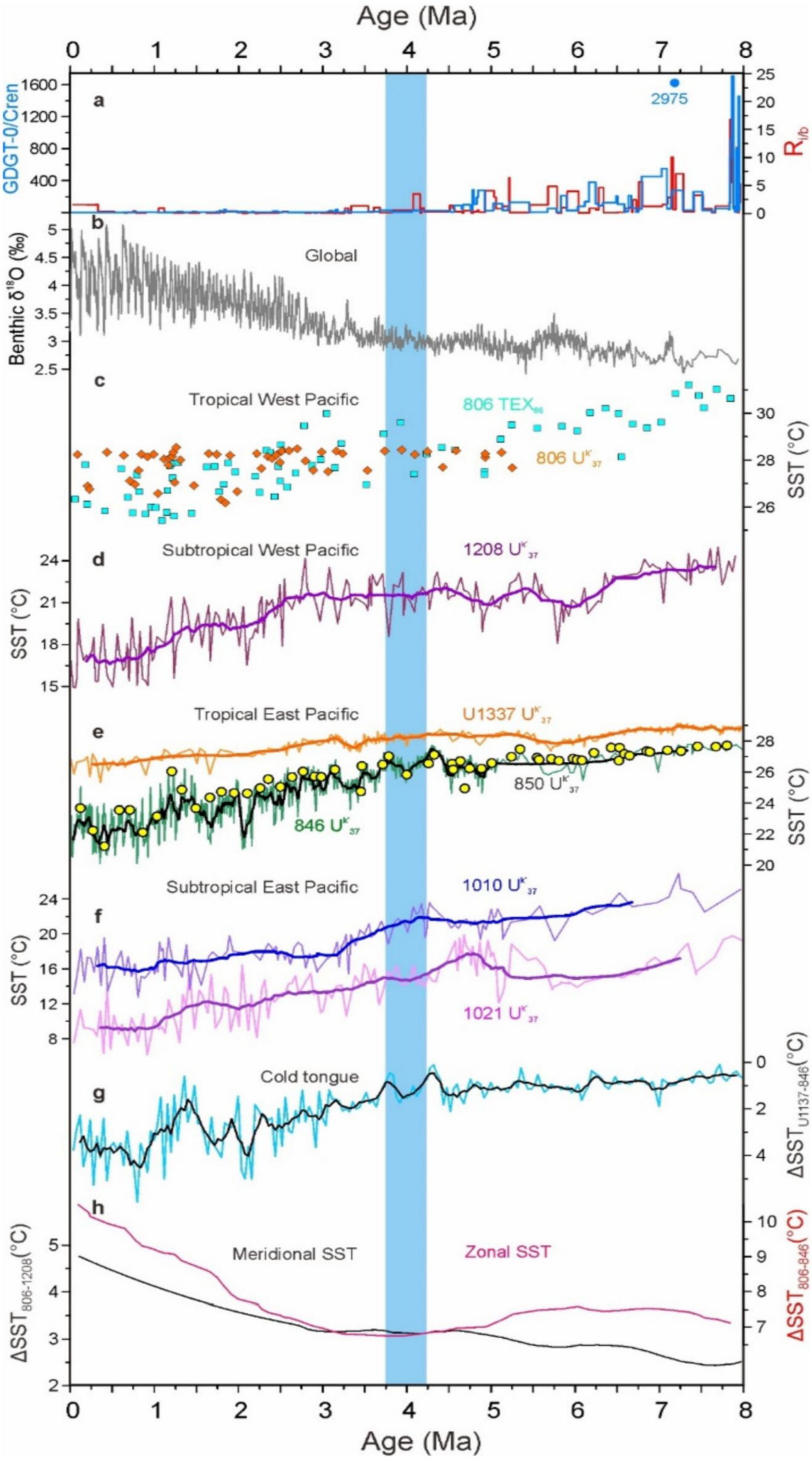

Fig3. Temperature evolution of the tropical and midlatitude Pacific since 8 Ma. a, GDGT-0/Cren and Ri/b records from the NCP. b, Global benthic foraminifera δ18O record (Lisiecki and Raymo, 2005; Zachos et al., 2001). c, Records of the tropical West Pacific SST derived from TEX86 (cyan square) (Zhang et al., 2014) and Uk 37 (orange diamond) (Pagani et al., 2010). d, Uk 37-SST of mid-latitude West Pacific (LaRiviere et al., 2012). e, Alkenone-derived records tropical East Pacific

SST from ODP 846 (green curve) (Herbert et al., 2016; Lawrence et al., 2009), ODP 850 (yellow circle) (Zhang et al., 2014) and U1337 (orange curve) (Liu et al., 2019). f, Alkenonederived mid-latitude East Pacific SST records (LaRiviere et al., 2012): light purple, ODP 1021; blue curve, ODP 1010. g, Cold tongue development in the East Pacific (Liu et al., 2019) h, Zonal and meridional temperature gradients of the Pacific Ocean since 8 Ma (Zhang et al., 2014). See Fig. 7 for site locations.

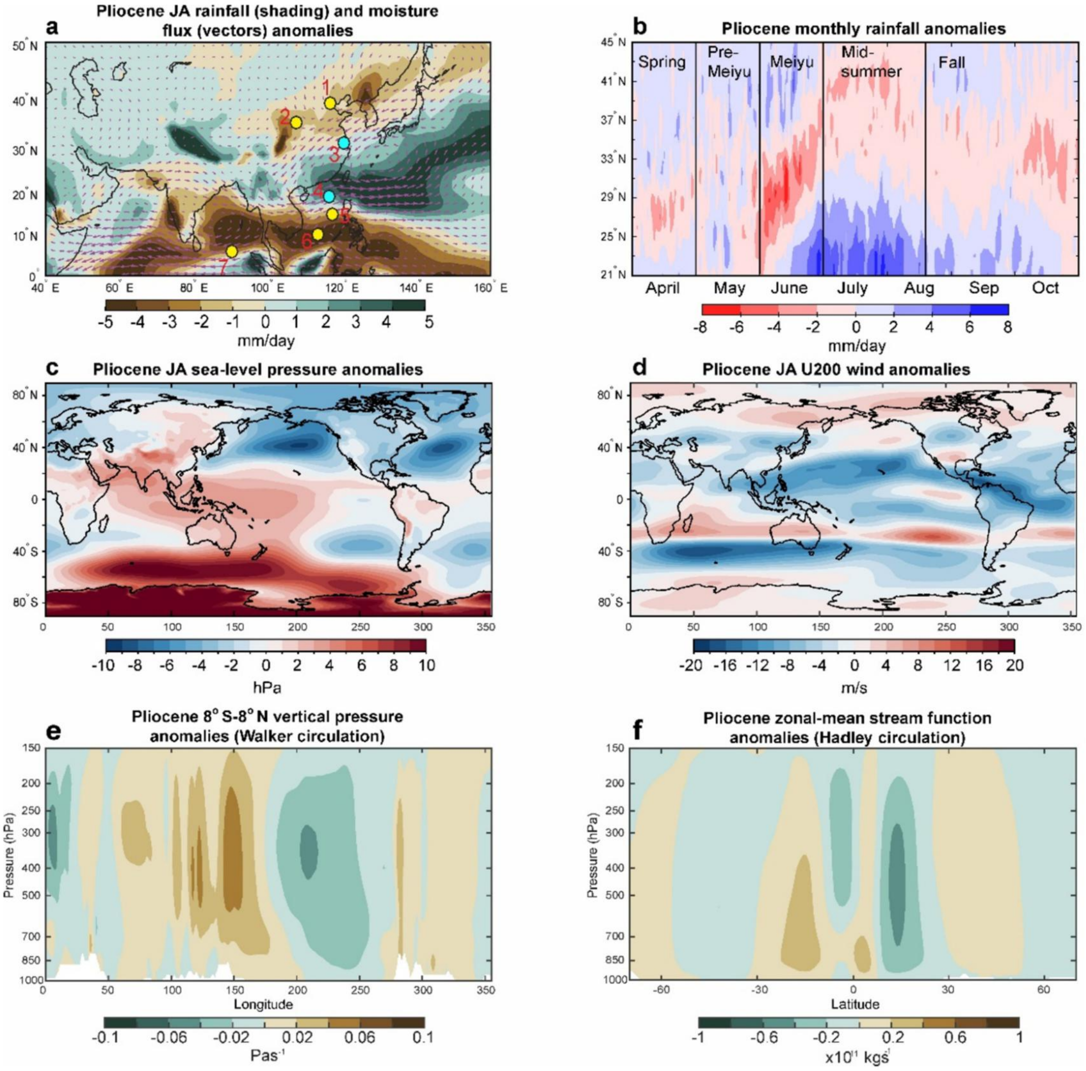

Fig4. Atmospheric circulation anomalies for the Pliocene minus preindustrial control run climate model simulations. a, July-August (JA) rainfall (shading) and moisture flux (vectors). Black symbols indicate the various study sites mentioned in the text (sites 1: North China Plain, this study; 2: Chinese Loess Plateau; 3, the lower reaches of the Yangtze River Valley; 4, the northern South

China Sea; 5, central South China Sea; 6, the southwestern South China Sea; 7, Bay of Bengal). b, Hovmöller diagram of precipitation anomalies over eastern China (110◦ to 125◦E). Approximate timings of the various intraseasonal stages are shown. c, JA sea-level pressure and d, 200 hPa zonal wind anomalies. e, JA vertical pressure velocity anomalies along the equator (computed as deviations from zonal mean and averaged between 8◦ S and 8◦ N) and f, zonal mean stream function. Brown (green) colors in e indicate anomalous downward (upward) flow, while brown (green) colors in f indicate counterclockwise (clockwise) flow.

2. 原位鉴别古新世-始新世极热事件沉积物中超大型针状磁小体

翻译人：蒋晓东 jiangxd@sustech.edu.cn

Wagner C L, Egli R, Lascu I, et al. ***In situ magnetic identification of giant, needle-shaped magnetofossils in Paleocene–Eocene Thermal Maximum sediments [J]****. PNAS, 2021, 118, 6.*

https://doi.org/10.1073/pnas.2018169118

摘要：新泽西威尔逊湖沉积物中古新世-始新世极热事件期间保存了丰富的超大型磁小体。我们发现这种超大的针状磁小体能够在低噪音、高分辨率一阶反转曲线（FORC）测试下产生独特的磁学信号，这一特征可用于全岩沉积物中鉴别这类超大型磁小体。基于透射电镜分析的超大型磁小体的微磁模拟也支持我们的结果。这些模拟强调了单畴特征、大矫顽力和极其拉长的晶体。超大型磁小体目前仅被发现于全球变暖事件的沉积物中，意味着可作为环境扰动记录的磁学标志物。因此我们提供了一种无损的 FORC 测试方法用以鉴别全岩沉积物中的超大型磁小体，也能够帮助评估他们的生态以及环境变化意义。

ABSTRACT: Near-shore marine sediments deposited during the Paleocene–Eocene Thermal Maximum at Wilson Lake, NJ, contain abundant conventional and giant magnetofossils. We find that giant, needle-shaped magnetofossils from Wilson Lake produce distinct magnetic signatures in low-noise, high-resolution first-order reversal curve (FORC) measurements. These magnetic measurements on bulk sediment samples identify the presence of giant, needle shaped magnetofossils. Our results are supported by micromagnetic simulations of giant needle morphologies measured from transmission electron micrographs of magnetic extracts from Wilson Lake sediments. These simulations underscore the single domain characteristics and the large magnetic coercivity associated with the extreme crystal elongation of giant needles. Giant magnetofossils have so far only been identified in sediments deposited during global hyperthermal events and therefore may serve as magnetic biomarkers of environmental disturbances. Our results show that FORC measurements are a nondestructive method

for identifying giant magnetofossil assemblages in bulk sediments, which will help test their ecology and significance with respect to environmental change.

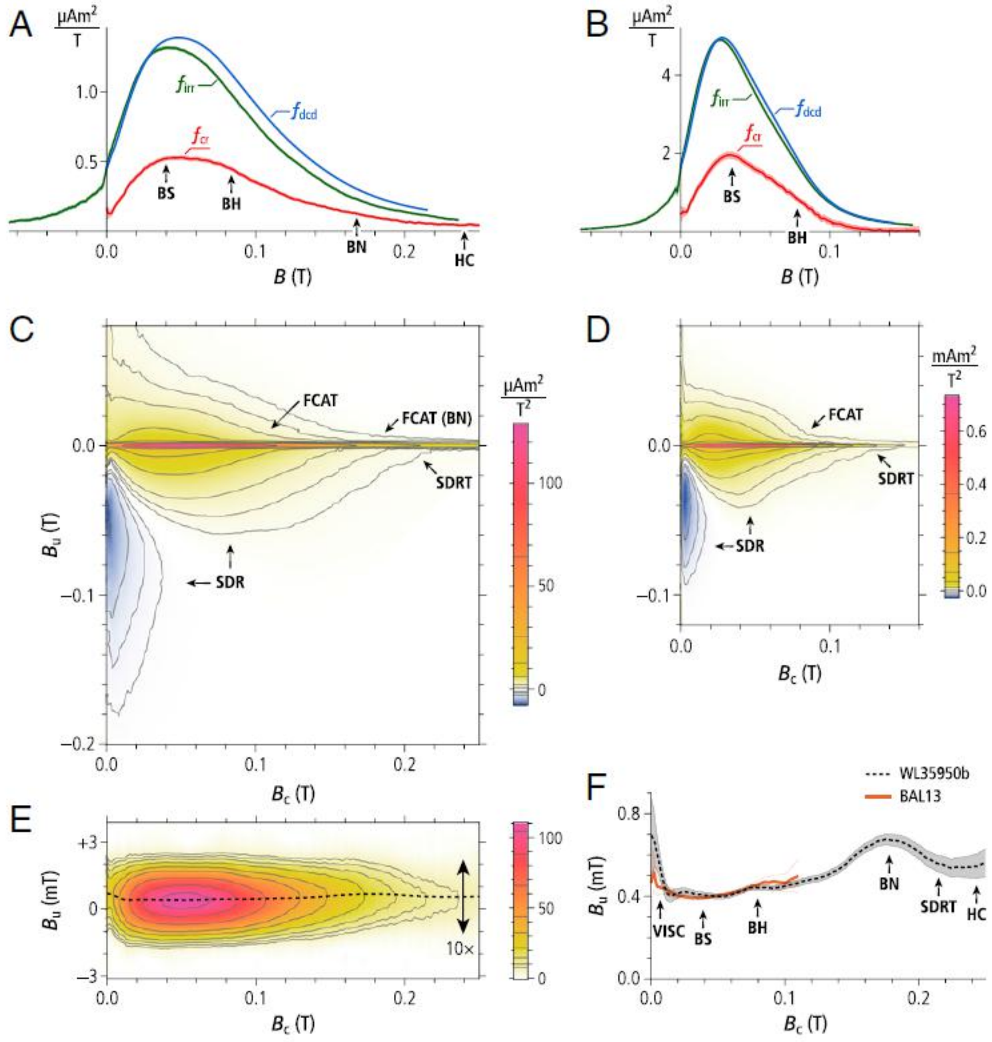

Fig1. Low-noise, high-resolution FORC measurements for WL35950b and BAL13. (A) Three distinct coercivity distributions identified in WL35950b. Arrows indicate the coercivity components BS (biogenic soft), BH (biogenic hard), BN (biogenic needles), and HC (high coercivity). (B) Same as A for BAL13. (C) FORC diagram for WL35950b. Arrows point to the following features: doublet of positive and negative amplitudes produced by reversible magnetic moment rotation in uniaxial SD (single-domain) particles (SDR); high-coercivity SDR termination (SDRT); high-coercivity termination of flux closure annihilation (FCAT) from particles and/or aggregates of particles (clumps, collapsed chains) with vortex-like magnetization states; and FCAT for biogenic needles

(FCAT [BN]). (D) FORC diagram for BAL13, plotted to scale with C. (E) Isolated central ridge contribution to the FORC diagram of WL35950b, with 10× vertical exaggeration highlighting the vertical offset with respect to $B_u = 0$. The dashed line is the expected Bu value for each vertical profile of the central ridge. (F) Vertical central ridge offset for WL35950b (dashed line) and BAL13 (solid line) Bc, with 1σ confidence intervals (shaded). These offsets are related inversely to the thermal activation volume of SD particles. Arrows point to coercivity ranges dominated by viscous particles (VISC), biogenic particles (B_S, B_H, and B_N), and high coercivity particles (HC). The SDRT marks the transition from biogenic to high-coercivity contributions.

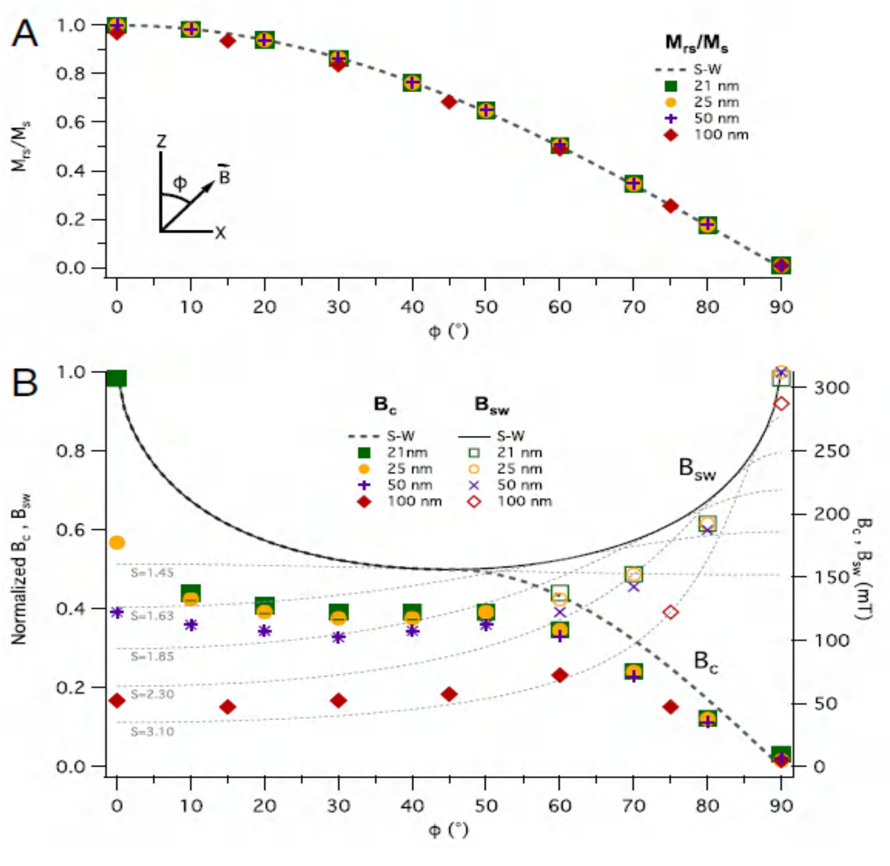

Fig 2. Summary of results from micromagnetic simulations on the 21-, 25-, 50-, and 100-nm-wide needles observed in magnetic extracts from WL35900 and WL35800 (50 and 100 nm) and inferred from our low-noise, high resolution FORC measurements (21 and 25 nm). Simulations were performed as a function of the angle (ϕ) between the applied field and the particle elongation direction, which was oriented in the z direction. The angular dependence was compared to Stoner–Wohlfarth (36) calculations for coherent rotation in an infinite cylinder (dashed and solid black lines,

S-W). (A) Magnetic squareness (Mrs/Ms) as a function of ϕ. The angular dependence follows the S-W model, Mrs/Ms (ϕ) = cosϕ. The dashed line is for Mrs/Ms (0°) = 1, which is the case for the 21- to 50-nm-wide needles (see also SI Appendix, Fig. S2). (B) Coercivity (Bc) and switching field (Bsw) as a function of ϕ. For $\phi < 60°$, the symbols for Bc and Bsw overlap. The gray dashed lines are calculations of the nucleation field for cases exhibiting fanning ($S \leqslant .1.63$) and curling ($S > 1.63$) of moments. S is a parameter that depends on particle width, exchange constant, and Ms (see SI Appendix, Text S2, for details of the theoretical calculations).

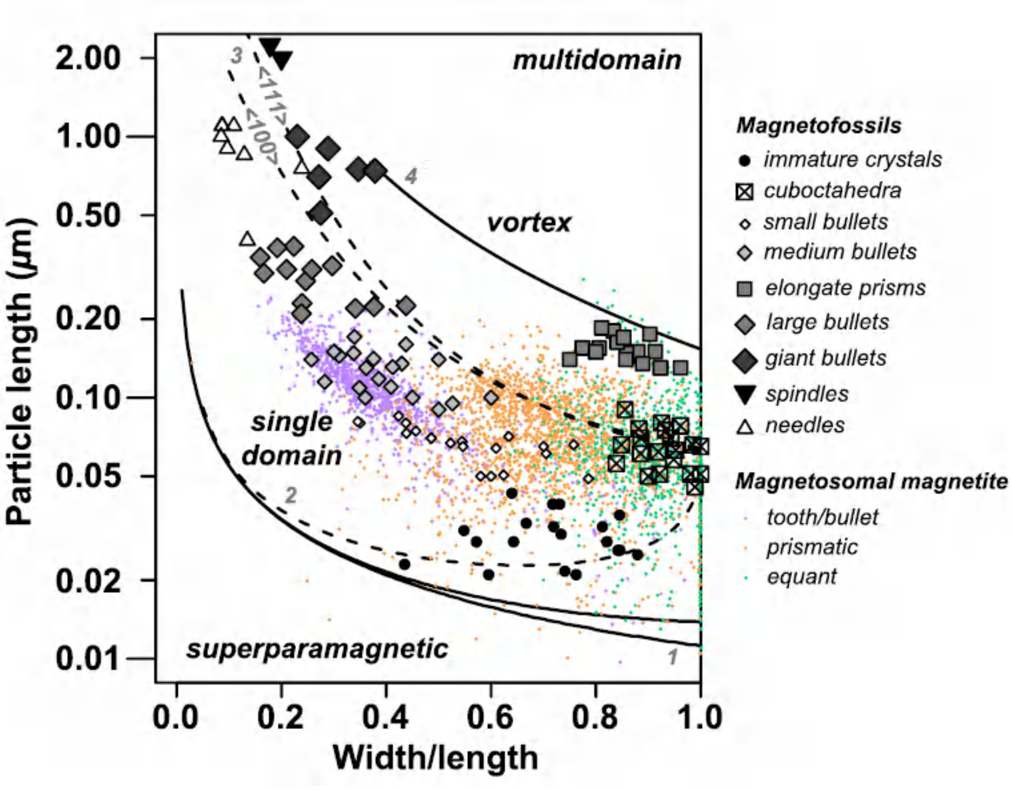

Fig 3. Dimensional analysis of magnetofossils identified in WL35900 and WL35800 with predicted domain states at room temperature. The theoretical single-domain states for individual grains and magnetofossil chains are highlighted: 1) lower limit for a six-crystal chain with intercrystal gaps of 0 (lower curve) and 0.6 times the length of constituent crystals (41), 2) lower limit for isolated single-domain particles (39), 3) upper limits for isolated single-domain particles with long axes parallel to the ⟨100⟩ and ⟨111⟩ crystallographic axes (40), and 4) critical sizes for isolated crystals within a chain of three crystals (40). Dimensions of modern magnetosomal magnetite of various shapes from well-characterized magnetotactic bacteria and conventional magnetofossils are shown

in color (for a complete list of data sources, see SI Appendix, Text S3).

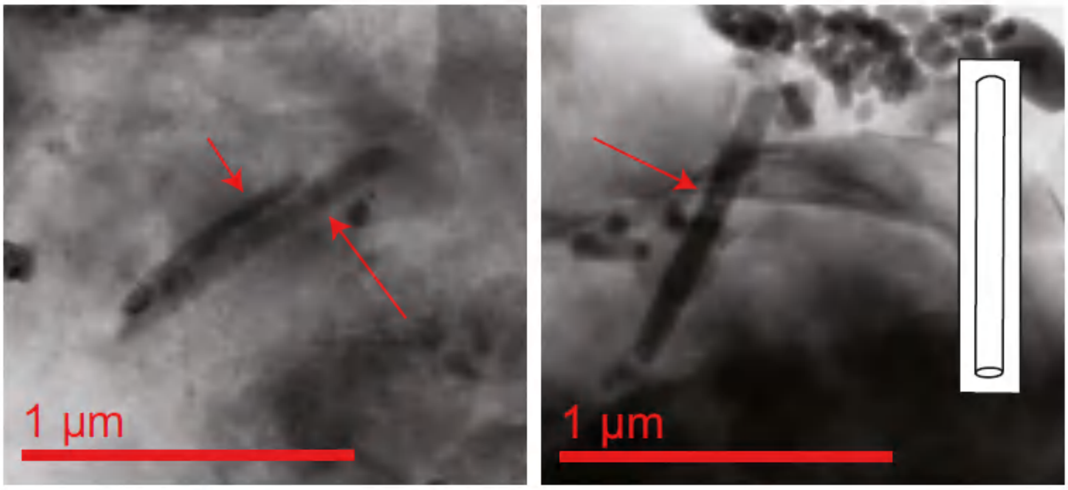

Fig 4. TEM images of giant needles from magnetic extract WL35900 highlighted with red arrows. Two needles are shown in the Left panel, whereas the Right panel shows a single needle with several conventional magnetofossils in the upper right. Needles have a cylindrical-like morphology (Inset in Right) and some taper toward one end of the crystal.

3. 俯冲的钠长石在水循环和俯冲流体碱性中的作用

翻译人：冯婉仪 fengwy@sustech.edu.cn

Huang G C, Hwang H, Bang Y, et al. ***A role for subducted albite in the water cycle and alkalinity of subduction fluids[J]****. Nature Communications, 2021, 12:1155.*

https://doi.org/10.1038/s41467-021-21419-6

摘要：钠长石是地壳的主要成分之一。在这里，我们报道了当钠长石发生含水冷俯冲时，会在高于 2.9 GPa 和 290 °C 或约 90 公里深度条件下，分解成含水的蒙脱石、斜硅石和刚玉，随后在高于 4.3 GPa 和 435 °C 或接近 135 公里的深度条件下，蒙脱石分解形成硬玉。水化成蒙脱石时，体系的流体体积减少了~ 14%，而当蒙脱石脱水成硬玉时，体系的流体体积增加了~ 8%。在过去的 5 年里，沿着南马里亚纳海沟，水化深度和脱水深度与地震活动的增加分别有 93%和 104%的相关性。此外，蒙脱石的形成伴随着 OH−的释放，这可以解释镁锰矿的形成和预期中俯冲流体的碱性。因此，我们对当代全球俯冲系统的水传输机制及相关地球化学和地球物理活动有了新的认识。

ABSTRACT: Albite is one of the major constituents in the crust. We report here that albite, when subjected to hydrous cold subduction conditions, undergoes hitherto unknown breakdown into hydrated smectite, moganite, and corundum, above 2.9 GPa and 290 °C or about 90 km depth conditions, followed by subsequent breakdown of smectite into jadeite above 4.3 GPa and 435 °C or near 135 km depth. Upon the hydration into smectite, the fluid volume of the system decreases by ~ 14 %, whereas it increases by ~ 8 % upon its dehydration into jadeite. Both the hydration and dehydration depths are correlated to increases in seismicity by 93 % and 104 %, respectively, along the South Mariana trench over the past 5 years. Moreover, the formation of smectite is accompanied by the release of OH− species, which would explain the formation of moganite and expected alkalinity of the subducting fluid. Thus, we shed new insights into the mechanism of water transport and related geochemical

and geophysical activities in the contemporary global subduction system.

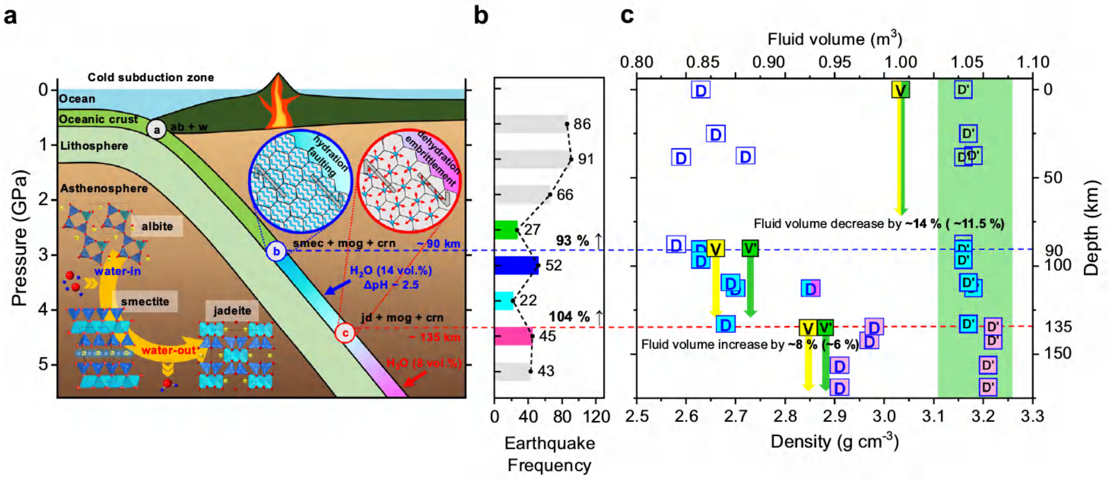

Fig1. The breakdown model of albite along the South Mariana trench. a The hydration and dehydration breakdowns of albite occur at ca. 90 km and 135 km depths, respectively. b The frequency of earthquake occurrence along the South Mariana trench over past 5 years (ISC Bulletin, investigation period between Nov. 2014 and Nov. 2019). c Changes in the net crystalline density (D for albite, D' for basalt) and fluid volume (V for albite, V' for basalt) in the subducting system are estimated as a function of subducting depth as in a and b. Green arrow and region highlight the estimated changes based on a basalt system. Phase abbreviations: albite: ab; smectite: smec; moganite: mog; corundum: crn; jadeite: jd; and water: w.

4. 来自 6 百万年长的钼同位素记录为大洋缺氧事件（OAE2）期间全球地球化学循环提供新的约束

翻译人:李园洁 liyj3@sustech.edu.cn

Dickson A J, Jenkyns H C, Idiz E, et al. ***New Constraints on Global Geochemical Cycling During Oceanic Anoxic Event 2 (Late Cretaceous) From a 6-Million-year Long Molybdenum-Isotope Record[J]****. Geochemistry, Geophysics, Geosystems, 2021, 22(3): e2020GC009246.*

https://doi.org/10.1029/2020GC009246

摘要：据推测，极端暖期可能会导致大洋中的氧气含量下降。显生宙地质记录到短期（<100 万年）内大洋缺氧达到顶峰称为大洋缺氧事件（OAEs），大洋缺氧事件证实了这个推测。但是跨越大洋缺氧事件之前和之后几个百万年的数据非常缺乏。本文作者展示了南德克萨斯州 Eagle Ford 组的石灰岩和泥灰岩的钼同位素记录，该记录于白垩纪北美西部内陆航道 6 百万年内包括 OAE2（森诺曼阶晚期-土仑阶早期，~94 Ma）沉积的。OAE2 之前厌氧环境下形成沉积物中的 Mo 同位素成分表明古海水组成限制为 1.1%-1.9%。这个值与之前仅在原北大西洋沉积的硫化物沉积物中确定的 OAE2 峰值的~1.5%相近。Mo 同位素在晚显生宙的全球缺氧的最极端事件之一过程中变化不到百万分之几。作者认为新的数据反映的不是大洋缺氧过程中有限的变化，而是与玄武岩-海水相互作用，大陆风化和部分氧化的浅海陆架有关的全球铁循环。这些过程对同位素轻的钼的埋藏具有重要作用，因而起到平衡其移动到硫化物沉积物中。

ABSTRACT： Intervals of extreme warmth are predicted to drive a decrease in the oxygen content of the oceans. This prediction has been tested for the acme of short (<1 million years) episodes of significant marine anoxia in the Phanerozoic geological record known as Oceanic Anoxic Events (OAEs). However, there is a paucity of data spanning prolonged multimillion-year intervals of geological time before and after OAEs. We present a Mo-isotope record from limestones and marlstones of the Eagle Ford Group, South Texas, which was deposited in the southern Cretaceous Western

Interior Seaway of North America during a 6-million-year period encompassing OAE 2 (Late Cenomanian-early Turonian: ~94 Ma). Mo-isotope compositions from deposits that formed in euxinic (sulfidic) conditions before OAE 2 allow the paleo-seawater composition to be constrained to 1.1%-1.9%. This range of values overlaps previous estimates of up to ~1.5% for the peak of OAE 2 determined from similarly sulfidic sediments deposited in the restricted proto-North Atlantic Ocean. Mo-isotopes thus varied by less than a few tenths of per mil across one of the most extreme intervals of global deoxygenation in the Late Phanerozoic. Rather than a limited change in oceanic deoxygenation, we suggest that the new data reflect changes to global iron cycling linked to basalt-seawater interaction, terrestrial weathering and expanded partially oxygenated shallow shelf-seas that played a key role in the burial of isotopically light molybdenum, thus acting as a counterbalance to its removal into sulfidic sediments.

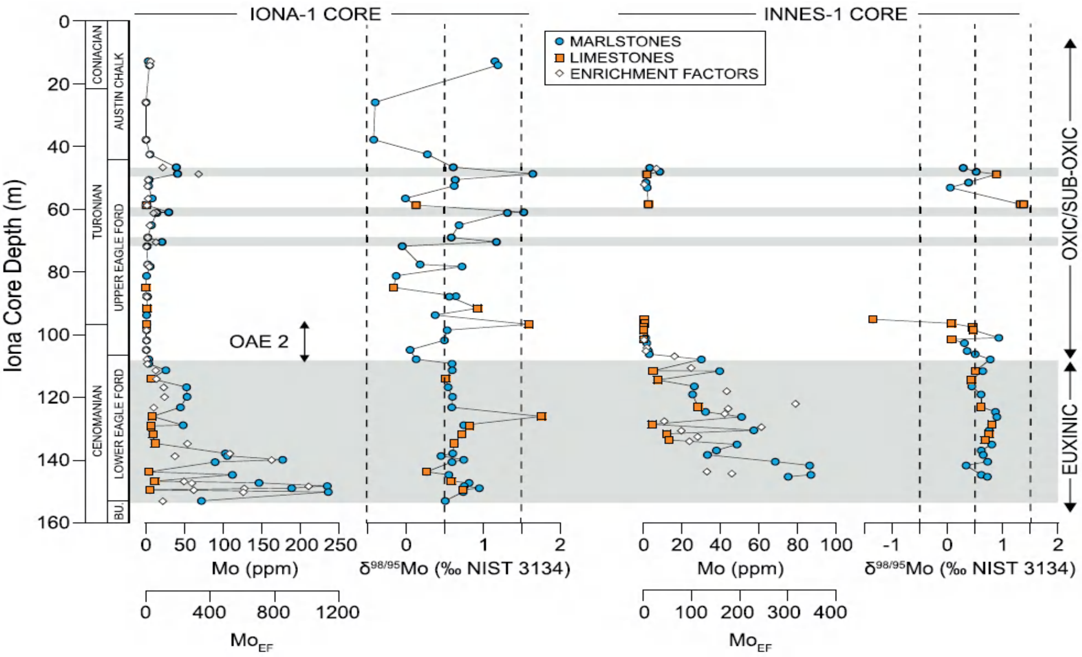

Fig 1. $\delta^{98/95}$Mo and Mo concentration data from the Iona-1 and Innes-1 cores. Data are delineated by lithology. Vertical dashed lines are to enable visual comparison between the Mo-isotope data for each core. Zones of reduced oxygenation, including the Lower Eagle Ford and intervals in the Upper Eagle Ford, are highlighted by gray shading.

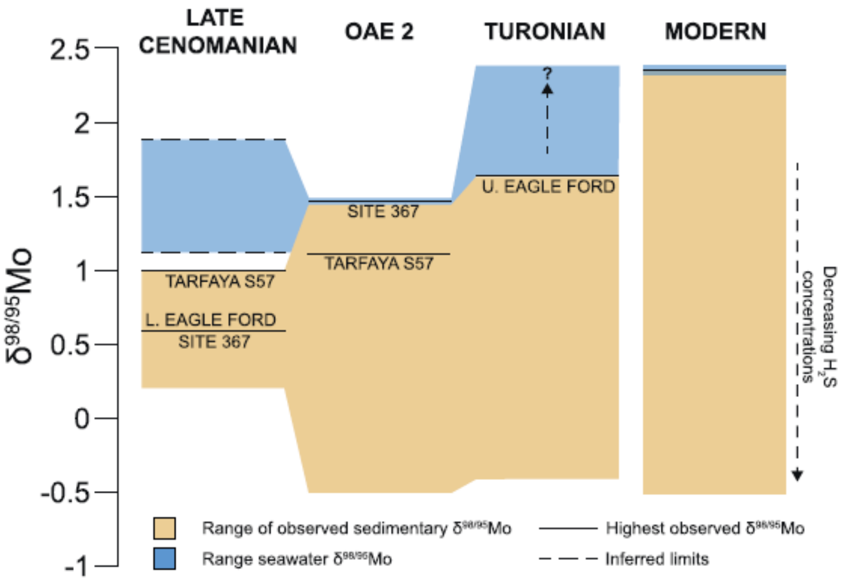

Fig 2. Constraints on the $\delta^{98/95}$Mo composition of Late Cretaceous and modern seawater. Solid horizontal lines indicate highest $\delta^{98/95}$Mo values observed from sediments accumulating in euxinic waters in restricted or nonrestricted marine basins (Westermann et al., 2014; Dickson et al., 2016; Goldberg et al., 2016; this study). The range of $\delta^{98/95}$Mo for all sediments measured in each time slice is represented by the yellow shading (Lower Cenomanian: 0.2%–1% (Site 367, S57 and Iona-1, Westermann et al., 2014; Dickson et al., 2016; Goldberg et al., 2016); OAE-2: −0.5%–1.5%, (Site 367, S57 and Site 1,276, Westermann et al., 2014; Dickson et al., 2016; Goldberg et al., 2016); Turonian: −0.4%–1.6% (Iona-1). The possible range of seawater $\delta^{98/95}$Mo for each time slice is indicated by the blue shading. Inferred limits on the range of seawater $\delta^{98/95}$Mo are indicated by horizontal dashed lines. The vertical dashed line indicates that the seawater composition for the Turonian extends above the highest measured sediment $\delta^{98/95}$Mo value by an unknown amount. The modern sediment data range is from Siebert et al., 2003, 2006; Neubert et al., 2008; Poulson-Brucker et al., 2009; Nägler et al., 2011; Nakagawa et al., 2012; Noordmann et al., 2015; Hardisty et al., 2016; Scholz et al., 2017; Brüske et al., 2020.

5. 公元前一千年来的地磁轴向偶极子变化——基于西欧新的古地磁数据和全球古地磁方向数据分析

翻译人：柳加波 liujb@sustech.edu.cn

Hervé G, Chauvin A, Lanos P, et al. ***How did the dipole axis vary during the first millennium BCE? New data from West Europe and analysis of the directional global database[J]****. Physics of the Earth and Planetary Interiors, 2021: 106712.*

https://doi.org/10.1016/j.pepi.2021.106712

摘要：我们对公元前一千年欧洲的地磁场长期变化有个一定的了解。但是，早期的古地磁数据仍然不足，尤其是位于中地中海区域。本文研究了公元前 13-4 世纪来自法国和意大利的考古窑、陶器和烤制的粘土碎片等，获得了新的三个古方向和六个古强度数据。古地磁数据通过热退磁的方法测量。古强度数据使用了 Thellier-Thellier 方法，并且校正了各向异性和冷却速率的影响。这些新的古地磁数据证实了公元前 1000-500 年欧洲存在的快速地磁场变化，即较高的地磁场强度伴随着较大轴向偶极子场方向漂移。这期间的另一个显著特征是虚拟地磁极的位置和欧洲以及中东的结果存在 25°左右的径向差异。这种不同寻常的变化可能主要受到黎凡特异常（Levantine Iron Age anomaly, LIAA）从中东向欧洲扩张的影响。然而，通过回顾公元前 1000 至 600 年的全球古地磁方向数据库（其中 96％来自欧洲、中东、东亚、北美和夏威夷），几乎所有的虚拟地磁极的位置都与位于俄罗斯的自转轴偏移 10-25°。平均整体的虚拟地磁极曲线表明，地磁北极在此期间呈顺时针运动，并且偶极子倾斜了近 14°。这项研究表明，偶极子的倾斜可能是欧亚大陆西部地磁场快速变化的重要因素，尽管这种变化也可能受到了来自 LIAA 相关的非偶极子场作用。

ABSTRACT: Despite progress in the knowledge of secular variation during the first millennium BCE in Europe, data coverage remains poor at the earliest periods, especially in some regions as in the Central Mediterranean area. This study presents three new directional and six new intensity data between the 13th and the 4th centuries BCE on archaeological kilns, pottery and baked clay fragments from South Italy and

France. Archaeodirections were determined after thermal demagnetizations and archaeointensities using the Thellier-Thellier protocol with corrections for the anisotropy and cooling rate effects. The new data confirm the large deviation of the direction from a Geocentric Axial Dipole field, the high geomagnetic field strength and the fast secular variation observed in Europe during the earliest half of the first millennium BCE. Another characteristic of this period is a difference of ~25° between the longitudes of the virtual geomagnetic poles inferred from European and Middle East data. This unusual behaviour can be mainly related to the Levantine Iron Age anomaly (LIAA) and its expansion from the Middle East to Europe. However, the review of the global directional database shows that almost all virtual geomagnetic poles, 96% of them coming from Europe, the Middle East, East Asia, North America and Hawaii, are 10–25° away from the rotation axis towards North Russia between 1000 and 600 BCE. The calculation of a mean global VGP curve suggests that the North geomagnetic pole followed a clockwise motion during this period with a dipole tilt up to around 14°. This study shows that a dipole axis tilt may have played an important role in the rapid secular variation in western Eurasia, although part of this variation may also be related to non-dipole fields associated with the LIAA.

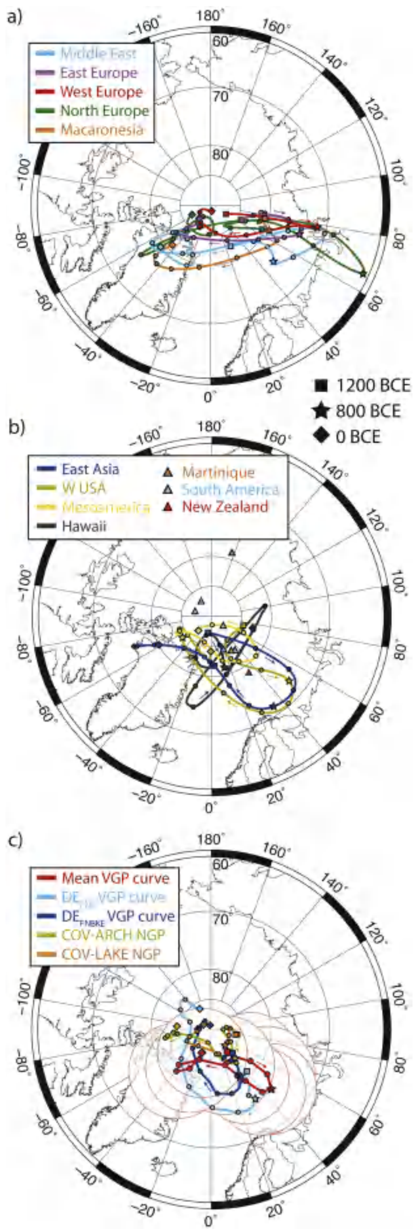

Fig. 1. Position of the virtual geomagnetic poles (VGP) from 1200 BCE (square symbols) to 0 BCE (diamond symbols). The star highlights the points at 800 BCE. (a) Mean VGPs curves from the Middle East, East Europe, West Europe, North Europe and Macaronesia. (b) Mean VGPs curves from East Asia, West USA, Mesoamerica and Hawaii plotted with individual data from other parts of the globe dated in the first half of the first millennium BCE. The Mesoamerican curve starts in 800 BCE instead of 1200 BCE. (c) Mean global VGP curve (red with Fisherian α95 confidence circles in transparency, this study) compared with DEFNBKE (dark blue) and DEFNB (light blue) mean curves built from sedimentary records (Nilsson et al., 2010) and with the positions of the North geomagnetic pole (NGP) predicted by spherical harmonic global models COV-ARCH and COV-LAKE (light green and orange, Hellio and Gillet, 2018).

6. 碎屑沉积揭示的东南亚大陆边缘巴拉望地块古地理

翻译人：周洋 zhouy3@sustech.edu.cn

Cao L C, Shao L, Qiao P J, et al. ***Formation and paleogeographic evolution of the Palawan continental terrane along the Southeast Asian margin revealed by detrital fngerprints [J].*** *Geological Society of America Bulletin, 2021, 133, 1167–1193.*

https://doi.org/10.1130/B35707.1

摘要：从中生代到新生代，东南亚大陆边缘长期微陆块会聚作用使该地区具有复杂的起源和构造演化阶段。在这些微陆块中，巴拉望地块地层的形成过程和古地理演化仍然存在不确定性和较大争议，尤其是在老地层的成岩作用以及与华南大陆边缘的共轭关系。本次研究从巴拉望和南海北部沉积盆地的中生代到新生代地层碎屑沉积（包括地球化学，重矿物和锆石 U-Pb 年代学）的角度探讨这些问题。物源对比以及使用最年轻的锆石年龄修订的地层框架为侏罗纪到中新世的区域古地理重建提供了新的视野。结果表明，物源的变化与巴拉望地块古地理相对应，从侏罗纪的增生复合体向新生代早期的裂谷边缘演化，最后到中新生代变为微陆块。根据物源特征对比，巴拉望地块被认为从中生代到渐新世，一直位于南海东北陆缘。从晚白垩世到新生代早期，巴拉望地块可能一直位于古南海的北缘，在渐新世—中新世，古南海洋壳俯冲并叠置于巴拉望地块之上。

ABSTRACT: The prolonged convergence along the Southeast Asian margin from the Mesozoic to Cenozoic shaped the region into a complex tectonic collage of microblocks of diverse origin and evolutionary history. Among these microblocks, the formation and paleogeographic evolution of the Palawan continental terrane remain issues of uncertainty and controversy, especially regarding the petrogenesis of the oldest rocks and the conjugate relationship with the South China margin. This study examined these issues from the perspective of detrital fngerprints (including geochemistry, heavy mineral, and zircon U-Pb geochronology) of Mesozoic to Cenozoic strata from Palawan

Island and basins of the northern South China Sea. The across-margin comparison of provenance signatures, favored by a comprehensive data compilation and a revision of the stratigraphic framework using the youngest zircon ages, provides insights into regional paleogeographic reconstructions from the Jurassic to the Miocene. The results reveal provenance shifts that correspond to the paleogeography of the Palawan continental terrane evolving from an accretionary complex in the Jurassic to a rifted margin in the early Cenozoic and finally to a microcontinent in the middle Cenozoic. Based on comparable provenance signatures, the terrane is interpreted to have been conjugated to the northeastern South China Sea margin from the Mesozoic until the Oligocene spreading of the South China Sea. The terrane likely existed as a northern passive margin of the proto–South China Sea from the latest Cretaceous to early Cenozoic before the oceanic crust of the latter was emplaced over the former during the Oligocene–Miocene.

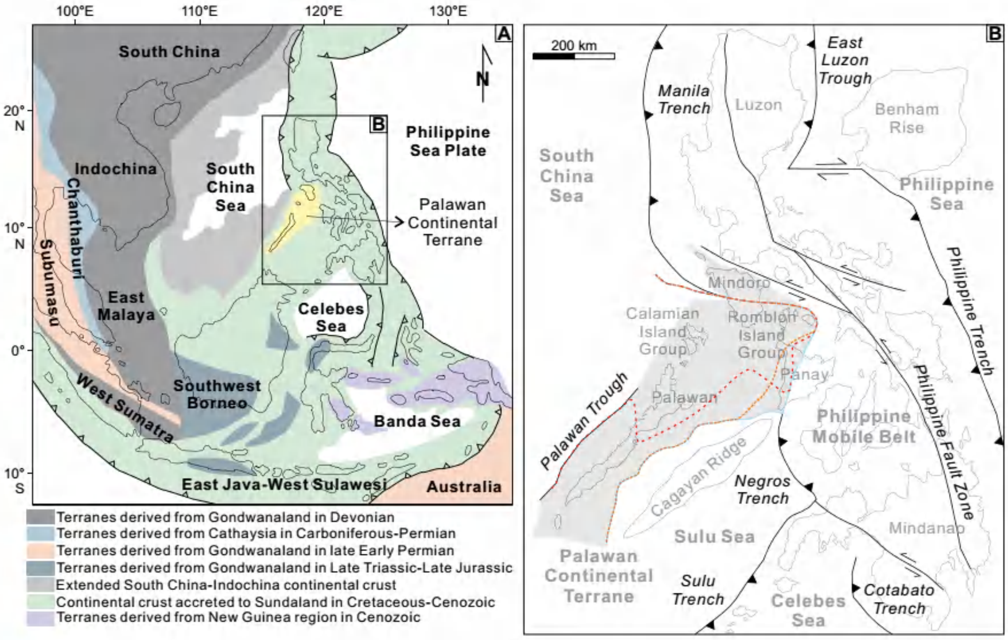

Fig1. (A) Present configuration of principal blocks in Southeast Asia showing the Palawan continental terrane located between the South China Sea and the Philippine Sea plate (modified from Metcalfe, 2013). (B) Tectonic map of the Philippines showing the Palawan continental terrane and Philippine mobile belt as well as different models regarding their common boundary. Gray shaded area is the extent of the Palawan continental terrane adopted in this study, which includes the islands

of Palawan, Calamian, Mindoro, Romblon, and west Panay (Canto et al., 2012; Gabo et al., 2015). Different parts of Palawan, Mindoro, and Panay are excluded in models marked by orange (Zamoras et al., 2008), red (Knittel et al., 2017; Liu et al., 2014), and blue (Concepcion et al., 2012; Gabo et al., 2009) lines.

7. 不同粒度磁铁矿的高温磁滞性质

翻译人：张琪 zhangq7@sustech.edu.cn

*Dunlop D. **Magnetic Hysteresis of Magnetite at High Temperature: Grain-Size Variation [J]. Geophysical Journal International**, 2021, ggab138（accepted）*

https://doi.org/10.1093/gji/ggab138

摘要：热剩磁作为火成岩的主要磁记忆，由高矫顽力和高解阻温度的载磁矿物在地质历史时期的稳定性决定。古地磁所记录的过去的地磁场方向和强度是揭示地球构造历史的关键。然而，我们对那些典型的可以记载稳定热剩磁的微米粒径尺度的磁铁矿，如何获得和保持磁信号的理解并不完全。高温环境下，磁铁矿的载磁能力和矫顽力的直接指标是 Mrs/Ms 的比值和矫顽力 Hc 值。本研究，首次测量了从室温到居里温度整个尺寸范围内，粒径从 25 nm 到 135nm 包含了超顺磁、单畴、假单畴和多畴属性的磁铁矿磁滞特性的变化。本文重点研究了 (1)Hc(T)和 Mrs(T)的观测结果及其重复性；(2)Hc(T)和 Mrs(T)与 Ms(T)的数学函数关系，用于建立 TRM 模型和对热变化进行无差比较；(3)退磁因子 N=Hc/Mrs 揭示磁铁矿晶粒的形状及其包含的磁畴数；(4)一般温度和升高温度情况下 Hc 和 Mrs 的粒度效应，描述磁畴结构变化和矫顽力机制。

ABSTRACT: Thermoremanent magnetization (TRM), the primary magnetic memory of igneous rocks, depends for its stability through geologic time on mineral carriers with high coercivities and high unblocking temperatures. The paleomagnetic record of past magnetic field directions and intensities is the key to unraveling Earth's tectonic history. Yet we still do not fully understand how the familiar mineral magnetite, in the micrometer grain size range typically responsible for stable TRM, acquires and holds its signal. Direct indicators of magnetite remanence-carrying capacity and coercivity at high temperature T are saturation remanence relative to saturation magnetization Mrs/Ms and coercive force Hc. This study is the first to measure the variation of these hysteresis properties for magnetite, from room temperature to the Curie point, across the entire size range from

25 nm to 135 µm, covering superparamagnetic, single-domain, vortex, pseudo-single-domain and multidomain magnetic behaviour. The paper focuses on: (1) Hc(T) and Mrs(T) observations and their reproducibility; (2) mathematical relationships of Hc(T) and Mrs(T) to Ms(T), used in modeling TRM and for unbiased comparisons of thermal variations; (3) the shapes of magnetite grains and the number of domains they contain, revealed by demagnetizing factors N = Hc/Mrs; and (4) the grain-size dependences of Hc and Mrs at ordinary and elevated T, delineating domain structure changes and mechanisms of coercivity.

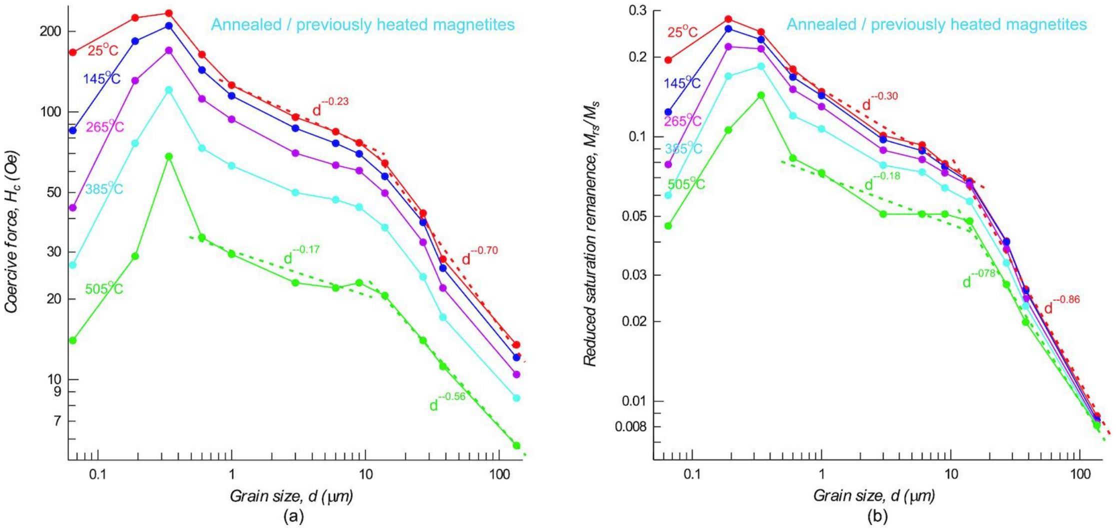

(a)

(b)

Fig1. Grain size dependences of (a) H_c and (b) M_{rs}/M_s data measured at selected temperatures between 25 ºC and 505 ºC. In the submicron range, values fall with decreasing size d because of broad size distributions in individual samples, which include much SP material with zero coercivity and remanence. In the 0.6 to 14 µm interval, the data are well described by power laws of $d^{-0.23}$ to $d^{-0.17}$ for H_c and $d^{-0.30}$ to $d^{-0.18}$ for M_{rs}/M_s. Above 14 µm, the descents are much steeper, with dependences of $d^{-0.70}$ to $d^{-0.56}$ for H_c and $d^{-0.86}$ to $d^{-0.78}$ for M_{rs}/M_s. N.B.1 Oe = 79.6 Am^{-1} (equivalent B: 10^{-4} T).

8. 一种变化关系的故事:全新世东亚夏季和冬季季风变化

翻译人：杨会会 11849590@mail.sustech.edu.cn

Kaboth-Bahr S, Bahr A, Zeeden C, et al. ***A tale of shifting relations: East Asian summer and winter monsoon variability during the Holocene[J]****. Scientific reports, 2021, 11(1): 1-10.*

https://doi.org/10.1038/s41598-021-85444-7

摘要：理解东亚夏季风(EASM)和冬季风(EAWM)之间的动态关系，是预测未来全球变暖情景下两者变化的必要条件。本文通过对东亚地区海相和陆相(非石笋)代用记录的叠加，探讨了 EASM 和 EAWM 之间的关系及其过去 10,000 年以来的变化机制。这为两个季风系统提供了区域和指标独立的信号。随后使用线性回归模型对各自的信号进行分析。我们发现 EASM 和 EAWM 之间的相位关系不是时间常数，明显依赖于轨道构型的变化。此外，大西洋经向翻转环流、北极海冰覆盖、ENSO 和太阳黑子数的变化也对全新世 EASM 和 EAWM 的千年尺度变化起着重要作用。我们还认为，由叠加的非石笋气候指标记录所捕获的季风活动的大部分信号支持了先前争论的石笋气候资料对水汽源变化和/或季节性的偏差。

ABSTRACT: Understanding the dynamics between the East Asian summer (EASM) and winter monsoon (EAWM) is needed to predict their variability under future global warming scenarios. Here, we investigate the relationship between EASM and EAWM as well as the mechanisms driving their variability during the last 10,000 years by stacking marine and terrestrial (non speleothem) proxy records from the East Asian realm. This provides a regional and proxy independent signal for both monsoonal systems. The respective signal was subsequently analyzed using a linear regression model. We find that the phase relationship between EASM and EAWM is not time constant and significantly depends on orbital configuration changes. In addition, changes in the Atlantic Meridional Overturning circulation, Arctic sea ice coverage, El Niño Southern Oscillation and Sun Spot numbers contributed to millennial scale changes in the EASM and EAWM during the Holocene. We also argue that the bulk

signal of monsoonal activity captured by the stacked non speleothem proxy records supports the previously argued bias of speleothem climatic archives to moisture source changes and/or seasonality.

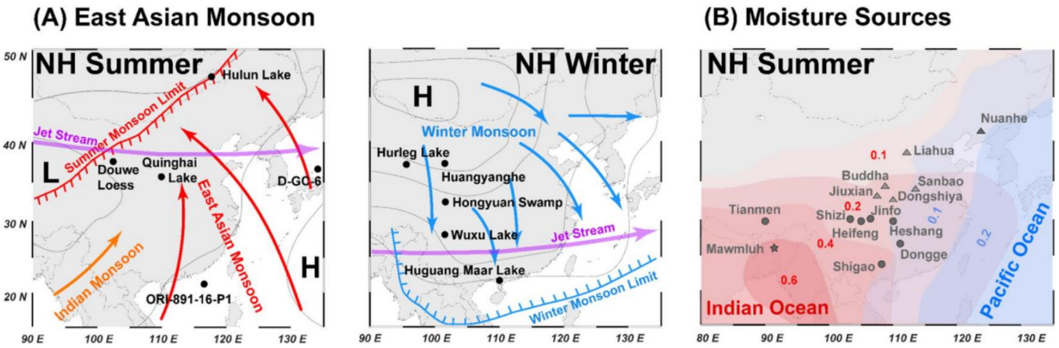

Fig1. East Asian summer (EASM) and winter monsoon (EAWM) purview and sites used for this study. (A) Atmospheric conditions during North Hemisphere summer (EASM). Northward propagating warm and moisture charged air masses are indicated by red arrows (left panel); Atmospheric conditions during North Hemisphere winter (EAWM). Southward trending cold air outbreaks are highlighted by blue arrows (right panel); (B) Moisture sources of East Asia during North Hemisphere summer (EASM). Numbers constitute relative contribution of the Indian Ocean (red) or Pacific Ocean (blue) moisture source to total amount of precipitation over East Asia. Sites used for the EASM and EAWM stack are marked by black dots in (A) and (B), respectively (Tables S1, S2). Purple arrow indicates position of the Jetstream. Location of the speleothem reference sites for the northern and southern Chinese speleothem stacks are marked by grey triangles and dots, respectively. Mawmluh speleothem cave site is marked with a grey star.

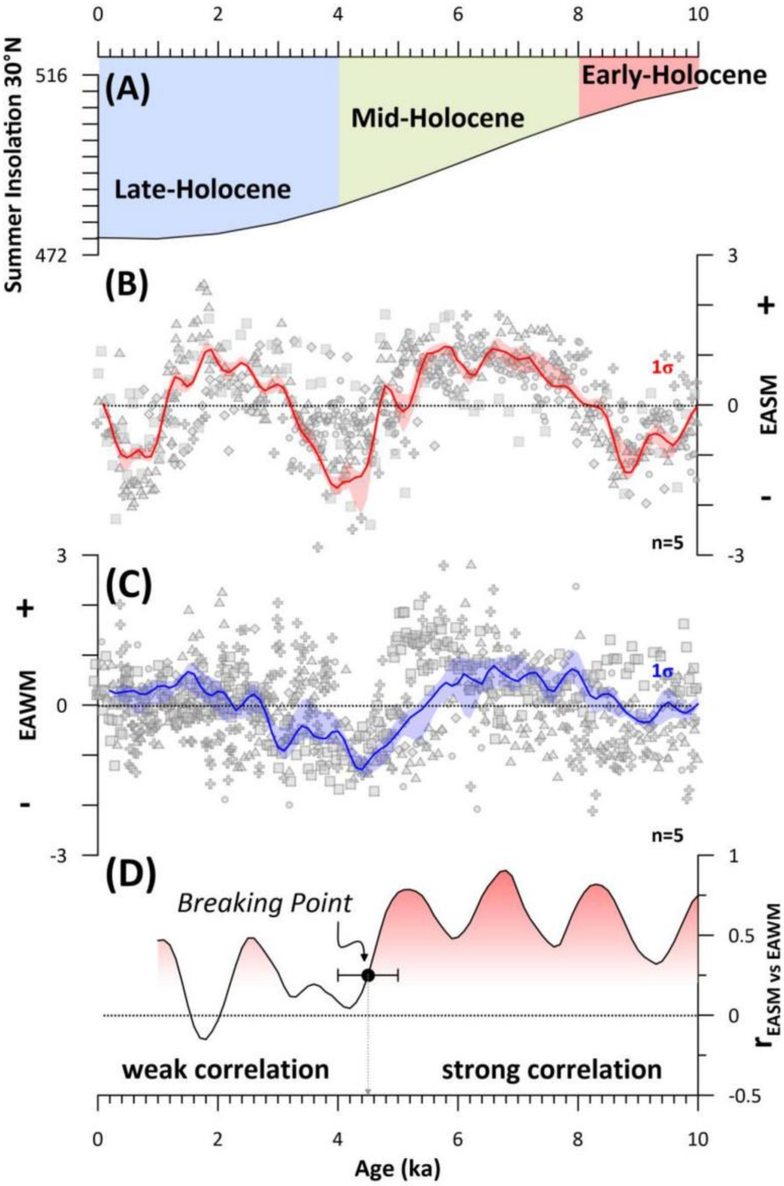

Fig2. East Asian summer (EASM) and winter (EAWM) monsoon stacks. (A) 21st June (summer) insolation for 30° N; The 2.5% and 97.5% (1 σ) uncertainty intervals for the stacks are shown as shaded (B) red (EASM) and (C) blue (EAWM) areas. The detrended original data sets used for each stack are marked by grey icons according to the Figure legend. (D) moving Spearman correlation coefficient (r) with window size = 1 between EASM and EAWM stacks. Shading indicates strong correlation (red) to weak correlation (white). The identified break point at 4.5 ± 0.5 kyr is indicated by a black dot with error bars.

9. 高分辨率磁测数据揭示的南海洋脊跃迁重新定向

翻译人：刘伟 inewway@163.com

Guan Q, Zhang T, Taylor B, et al. ***Ridge jump reorientation of the South China Sea revealed by high-resolution magnetic data[J].*** *Terra Nova.2021. online*

https://doi.org/10.1111/ter.12532

摘要：本文利用近年来采集到的南海东部次海盆的磁等时线资料，建立了南海东部次海盆的高分辨率磁等时线图，更新了南海东部次海盆海底扩张的时代，并揭示了一种新的洋脊重新定向。南海东部次海盆的海底扩张开始于 Chron 11n.1r (29.7 Ma)，在 Chron 5Br (15.6 Ma)停止扩张。连续的洋脊跃迁发生在 Chron 9r 和 7n 之间，这解释了南海东部次海盆的非对称几何结构。此外，与洋脊跃迁相关的洋脊重新定向指示了一种新的洋脊再定向模型，在该模型中洋脊离轴并同步重新定向以适应海底扩展的新方向。在南海东部次海盆中，这种类型的重新定向对板块运动方向变化的响应比渐进式的山脊旋转更快。

ABSTRACT: We establish a high-resolution magnetic isochron pattern in the East Subbasin (ESB) of the South China Sea (SCS) based on recently collected magnetic data, which provides an updated age of seafloor spreading in the ESB and reveals a new type of ridge reorientation. Seafloor spreading in the ESB initiated at Chron 11n.1r (29.7 Ma) and ceased shortly after Chron 5Br (15.6 Ma). Successive ridge jumps occurred between Chrons 9r and 7n, which explains the substantial asymmetric geometry of the ESB. Furthermore, the ridge reorientation associated with ridge jumps highlights a new ridge reorientation model in which the ridge jumps off-axis and reorients synchronously to adapt to the new direction of seafloor spreading. In the ESB, this type of reorientation responds more rapidly to changes in the direction of plate motion than gradual ridge rotation.

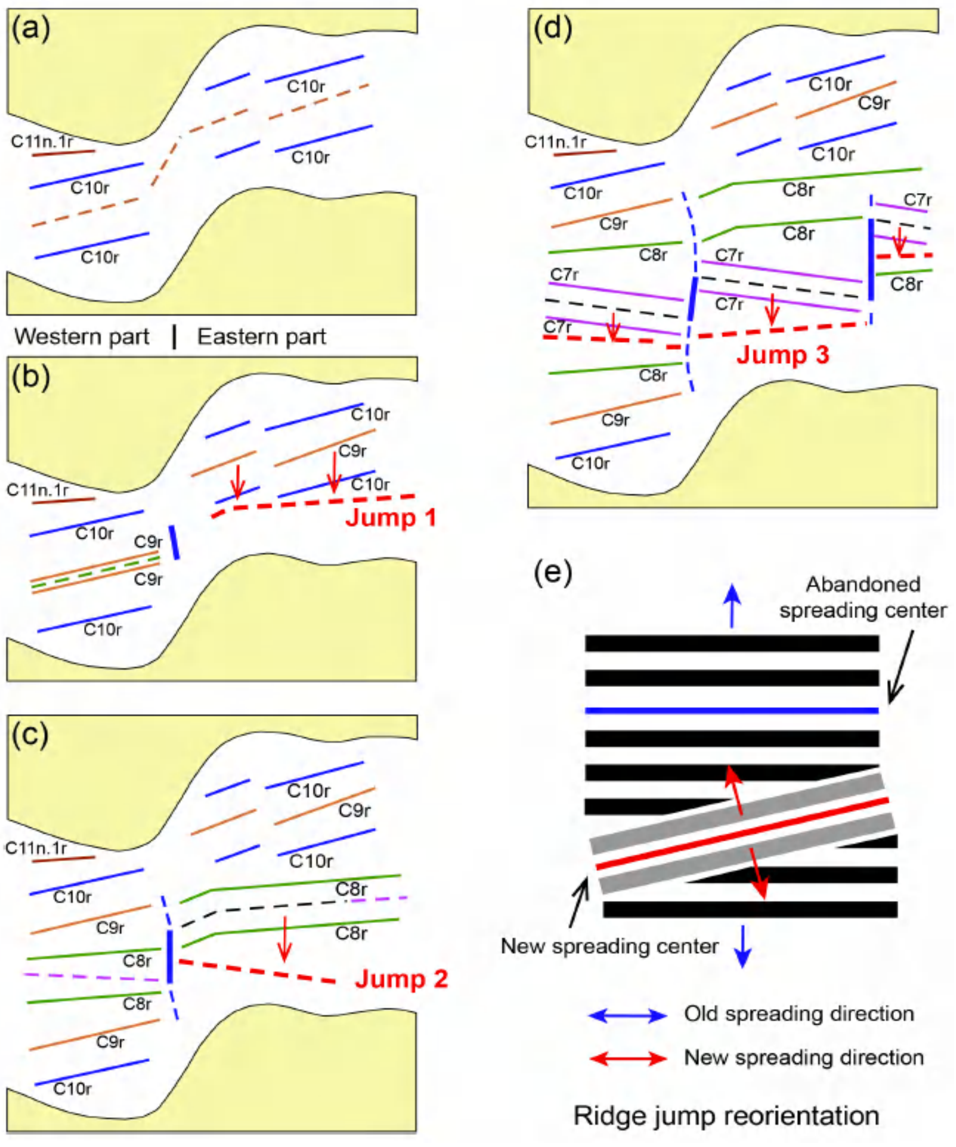

Fig 1. Schematic illustration of the ridge reorientation in the ESB. (a)–(d) The evolution of the spreading center and successive southward ridge jumps. The colored lines indicate the magnetic isochrons. The dashed red lines mark the new spreading center. The dashed black lines represent the fossil ridges. The red arrows show the directions of the ridge jumps. The thick blue lines denote the transform faults. The dashed blue lines are the fracture zones between the western and eastern parts. At the inception of seafloor spreading, the spreading center was discontinuous, and there was a non-transform discontinuity (NTD) between the western and eastern parts. After Chron 9r, the NTD was converted into a transform fault, which may be associated with the ridge jump J1. With the successive ridge jumps and continuous ridge reorientation, the transform fault eliminated at Chron 6Br. (e) Schematic model of the jump reorientation proposed in this study.

10. 一种用于火山监测和地质灾害评估的新型无人机磁测方法验证

翻译人：曹伟 11930854@qq.com

Lydie Gailler, Philippe Labazuy, Edouard Régis, Martial Bontemps, ***Thierry Souriot, Guillaume Bacques, and Bruno Carton. Validation of a New UAV Magnetic Prospecting Tool for Volcano Monitoring and Geohazard Assessment [J]****. Remote Sensing, 2021(13):894.*

https:// doi.org/10.3390/rs13050894

摘要：在火山环境中使用无人驾驶飞机（UAV）是研究火山和提高火山活动监测效率方面的一个关键挑战。无人机测量使地面和卫星测量在中等尺度上得到了加强。在进行可见光和红外测量的同时，无人机还可以进行地球物理测量以获得更深入的研究。磁场测量在火山环境中是一种强有力的工具，可用于（1）绘制不同年代或类型地层之间的构造关系图件，（2）深部热异常与侵入系统成像。本研究中，我们关注的是正在投入使用的磁传感器，特别是最近在轻型无人机上实现的标量系统，该系统可以在野外快速有效地部署。本文介绍了几种飞行试验结果，以讨论在磁测过程中无人机的伪影现象或环境条件，并且给出了无人机与地面同步测量的对比结果。我们证明了低空测量成像良好的磁异常与随时间变化的火山环境密切相关。此外我们还讨论了该技术在活火山探测和监测、火山 4D 成像等领域的应用前景。

ABSTRACT: The use of unmanned aircraft vehicles (UAVs) in volcanological contexts is a key challenge in studying volcanoes and improving efficiency in the monitoring of volcanic activity. The coupling of ground and satellite measurements has been reinforced at an intermediate scale thanks to UAV measurements. Along with carrying out visible and infrared measurements, UAVs can conduct geophysical measurements for more in-depth studies. Magnetic field measurements are a powerful tool in volcanic contexts for (i) mapping structural contacts between formations of different ages or type, and (ii) imaging deep thermal anomalies and intrusive systems. Here, we focus on magnetic sensors, which are becoming operational, and in particular

on a scalar system recently implemented on a light drone that can be deployed quickly and efficiently in the field. This paper presents several flight test results in order to discuss any artifacts of the UAV or environmental conditions in the magnetic measurements. The results of the comparison between simultaneous UAV and ground surveys are presented. We demonstrate that low altitude measurements are particularly relevant to well-imaged magnetic anomalies and their variation through time in a volcanic context. Some potential uses for this technology and associated applications are also discussed in the fields of exploring and monitoring active volcanoes, for the 4D imaging of volcanoes.

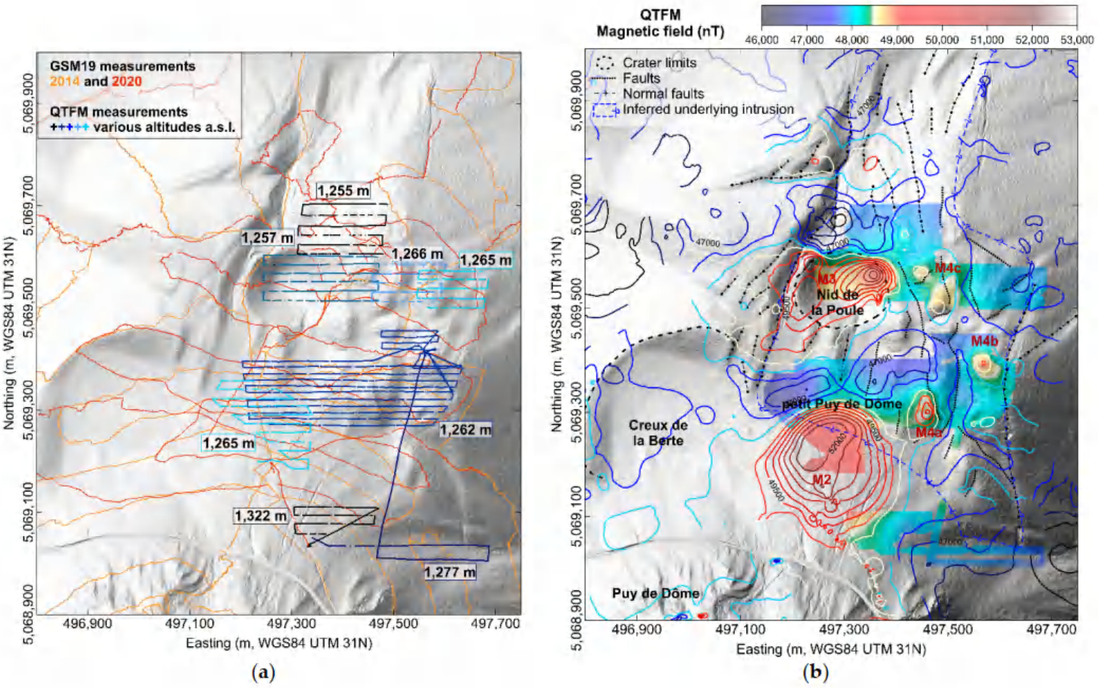

Fig 1. (a) Location of the magnetic measurements on the scale of the petit Puy de Dôme volcano. (b) QTFM total magnetic field interpolated and gridded at an averaged altitude (grid cell: 2 m). The GSM19 total magnetic field is superimposed as isocontours (500 nT spacing, same grid cell size and color scale).

11. 上新世温暖期间西风带的极移和减弱

翻译人：王敦繁 dunfan_w@foxmail.com

Abell J T, Winckler G, Anderson R F, et al. ***Poleward and weakened westerlies during Pliocene warmth[J]****. Nature, 2021, 589(7840):70-75.*

https://doi.org/10.1038/s41586-020-03062-1

摘要：盛行的中纬度西风，被称为西风，是气候系统的一个基本组成部分，因为它们在驱动海面环流和调节海气热量、动量和碳交换方面起着至关重要的作用。最近的研究表明，西风带正在向极地迁移，这是对人类活动的响应。重建过去温暖时期的西风带，比如上新世，当时大气中二氧化碳含量约为 350 至 450 ppm，温度比今天高 4 摄氏度，可以提高我们对随着气候变暖这些风系统的位置和强度变化的理解。我们的研究表明，在温暖的上新世，西风带比发生在大约 273 万年前的北半球冰川作用(iNHG)加强后的冰河期更弱，更倾向于向极地移动。在全球变暖期间，主要冰盖的发展伴随着中纬度北太平洋沙尘通量的显著增加，特别是与亚北极太平洋相比。在这一转变之后，风尘通量的变化很大程度上与上新世晚期和更新世早期的冰期-间冰期旋回有关。在此基础上，我们推断西风带的变化主要是由上新世-更新世温度梯度和冰量的变化引起的。结合其他风尘记录和气候模拟结果，我们发现西风带变化是全球同步的。如果上新世预示着未来的气候变暖，我们就可以假设西风带在两个半球间持续的向极移动和现在的减弱是可以预料的。

ABSTRACT: The prevailing mid-latitude westerly winds, known as the westerlies, are a fundamental component of the climate system because they have a crucial role in driving surface ocean circulation and modulating air–sea heat, momentum and carbon exchange. Recent work suggests that westerly wind belts are migrating polewards in response to anthropogenic forcing. Reconstructing the westerlies during past warm periods such as the Pliocene epoch, in which atmospheric carbon dioxide (CO_2) was about 350 to 450 parts per million6 and temperatures were about to 4 degrees Celsius

higher than today, can improve our understanding of changes in the position and strength of these wind systems as the climate continues to warm. Here we show that the westerlies were weaker and more poleward during the warm Pliocene than during glacial periods after the intensification of Northern Hemisphere glaciation(iNHG), which occurred around 2.73 million years ago .Our results, which are based on dust and export productivity reconstructions, indicate that major ice sheet development during the iNHG was accompanied by substantial increases in dust fluxes in the mid-latitude North Pacific Ocean, especially compared to those in the subarctic North Pacific. Following this shift, changes in dust and productivity largely track the glacial–interglacial cycles of the late Pliocene and early Pleistocene epochs. On the basis of this pattern, we infer that shifts in the westerlies were primarily driven by variations in Plio-Pleistocene thermal gradients and ice volume. By combining this relationship with other dust records and climate modelling results, we find that the proposed changes in the westerlies were globally synchronous. If the Pliocene is predictive of future warming, we posit that continued poleward movement and weakening of the present-day westerlies in both hemispheres can be expected.

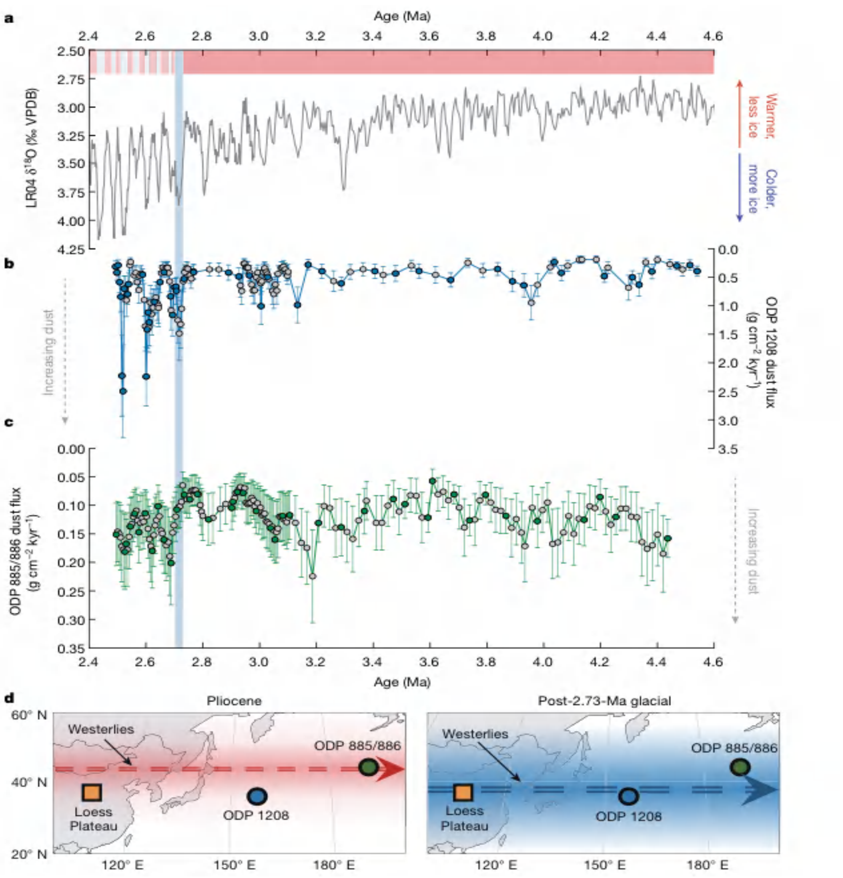

Fig1. Dust flux reconstructions from the Pliocene North Pacific indicate shifts in the westerlies after the iNHG. a, LR04 benthic oxygen isotope stack21 (VPDB, Vienna Pee Dee Belemnite). The dark red bar indicates the warm Pliocene before about 2.73 Ma, and the dark blue bar indicates the iNHG. Lighter red and blue bars show glacials and interglacials of the late Pliocene and early Pleistocene. b, Dust fluxes at ODP 1208. Blue filled circles indicate samples with measured 3HeET. c, Dust fluxes at ODP 885/886. Green filled circles indicate samples with measured 3HeET. In both dust records, dust fluxes were determined using Th concentrations and 3HeET-derived MARs. Error bars represent propagated analytical uncertainty for Th concentrations, along with analytical and statistical uncertainties for 3HeET-derived MARs (1σ). Arrows indicate colder/increased ice volume conditions and greater dust fluxes are downwards. Post-2.73-Ma peaks in dust flux at ODP 1208 are found during Marine Isotope Stages (MIS) G6, G4, G2, 104 and 100, and the dust values from these five glacials are used to determine dust amplification factors at the site. d, Schematic showing the hypothesized shift in the position and strength of westerlies from the Pliocene to glacials after the iNHG. Arrows represent the main axis of westerly winds, and the red- and blue-shaded regions indicate idealized dust plumes.

12. 西伯利亚莱文森-莱辛湖高纬度沉积物的矿物磁性特征

翻译人：张伟杰 12031188@mail.sustech.edu.cn

Scheidt S, Egli R, Lenz M, et al. ***Mineral Magnetic Characterization of high-latitude Sediments from Lake Levinson-Lessing, Siberia[J]****. Geophysical Research Letters.: e2021GL093026. https://doi.org/10.1029/2021GL093026*

摘要：中西伯利亚北部的莱文森-莱辛湖具有连续的、普遍恒定的高沉积速率的沉积记录。本研究首次证明了该湖沉积物 46 米长的 Co1401 岩心适合进行古地磁分析。虽然最底层 8 米被扰动，但 Co1401 上部 38 米被证明是一个优越的、高分辨率的古地磁记录的载体。通过对磁化率、非磁滞剩磁、等温剩磁和磁滞参数的高分辨率分析，可以看出矿物磁性性质基本一致。一阶反转曲线表明，假单畴磁铁矿颗粒是主要的剩磁载体，可能来源于趋磁细菌的单畴颗粒为次要的剩磁载体。在 6.7 m 以上，胶黄铁矿开始形成，整体矿物磁性比 6.7 m 以下稍硬一些。然而，主要的剩磁载体仍然是碎屑来源。

ABSTRACT: Levinson-Lessing Lake in northern Central Siberia is a sedimentary archive characterized by continuous, widely constant sedimentation at high rates (0.7 m ka-1 for >32 ka). This study provides the first evidence of the suitability of the lake´s sediments for paleomagnetic analyses using the 46 m-long core Co1401. Although the lowermost 8 m are disturbed, the upper 38 m of Co1401 provide the preconditions for an exceptional, high-resolution paleomagnetic record located within the tangent cylinder of the inner core. High-resolution analyses of magnetic susceptibility, anhysteretic remanent magnetization, isothermal remanent magnetization, and hysteresis parameters show largely uniform mineral magnetic properties. First-order reversal curves indicate magnetite particles in pseudo-single domain state are the main remanence carrier, supplemented by single-domain particles, originating likely from magnetotactic bacteria. Above 6.7 m, the bulk magnetic mineralogy is slightly harder than below, and initial greigite formation occurs. However, the main remanence carriers

are still of detrital origin.

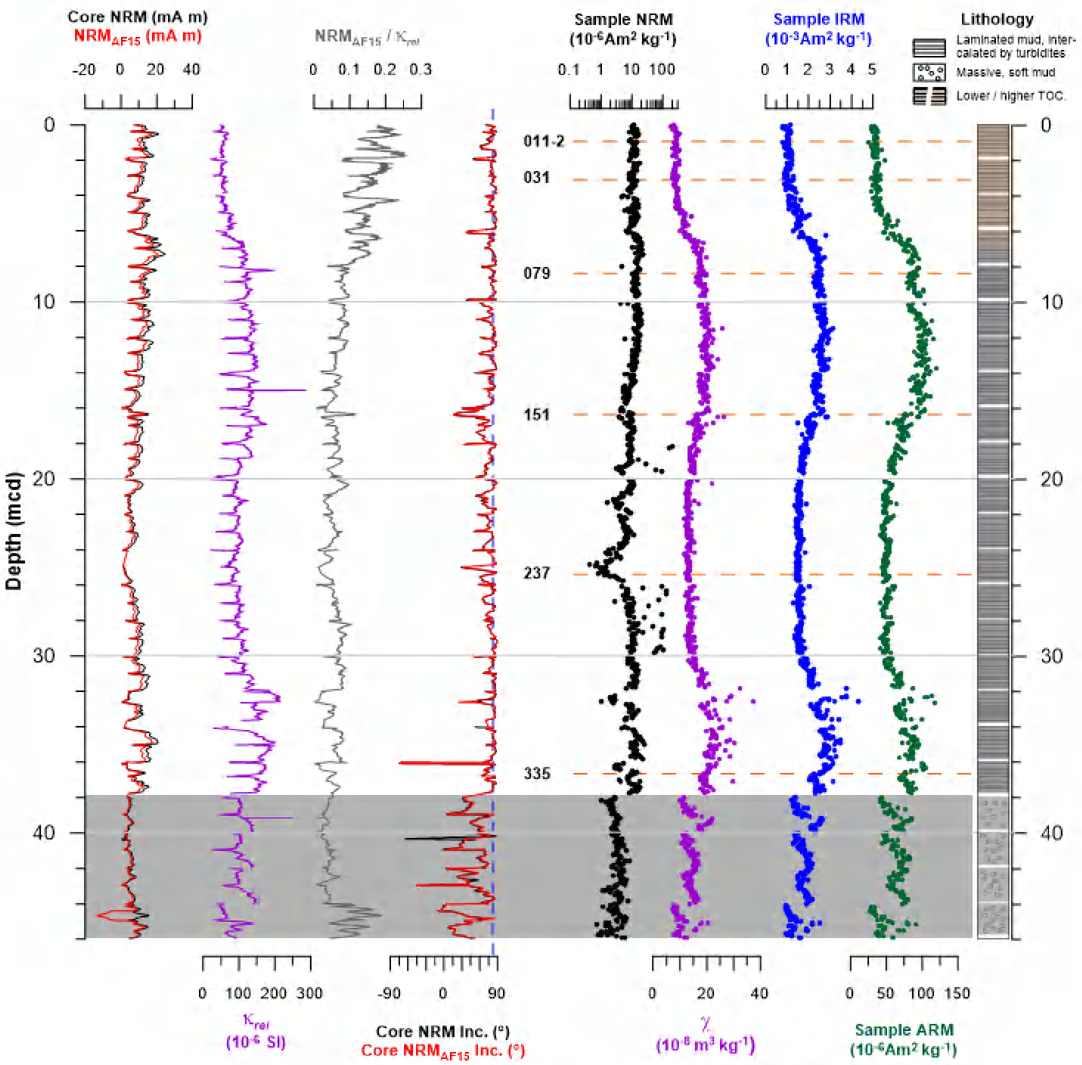

Fig1. Lithology and downcore plots of magnetic properties. Results of whole-core measurements (left): NRM, NRMAF15, κrel, NRM Inclination (NRM Inc.), NRMAF15 Inc. The blue vertical dashed line marks the 82.1° inclination expected for a GAD. Discrete sample measurement results (right): NRM, χ, IRM, ARM. Note the logarithmic scale for NRM. Samples shown in Figure 4 are marked by orange horizontal dashed lines. Grey background >38 mcd.

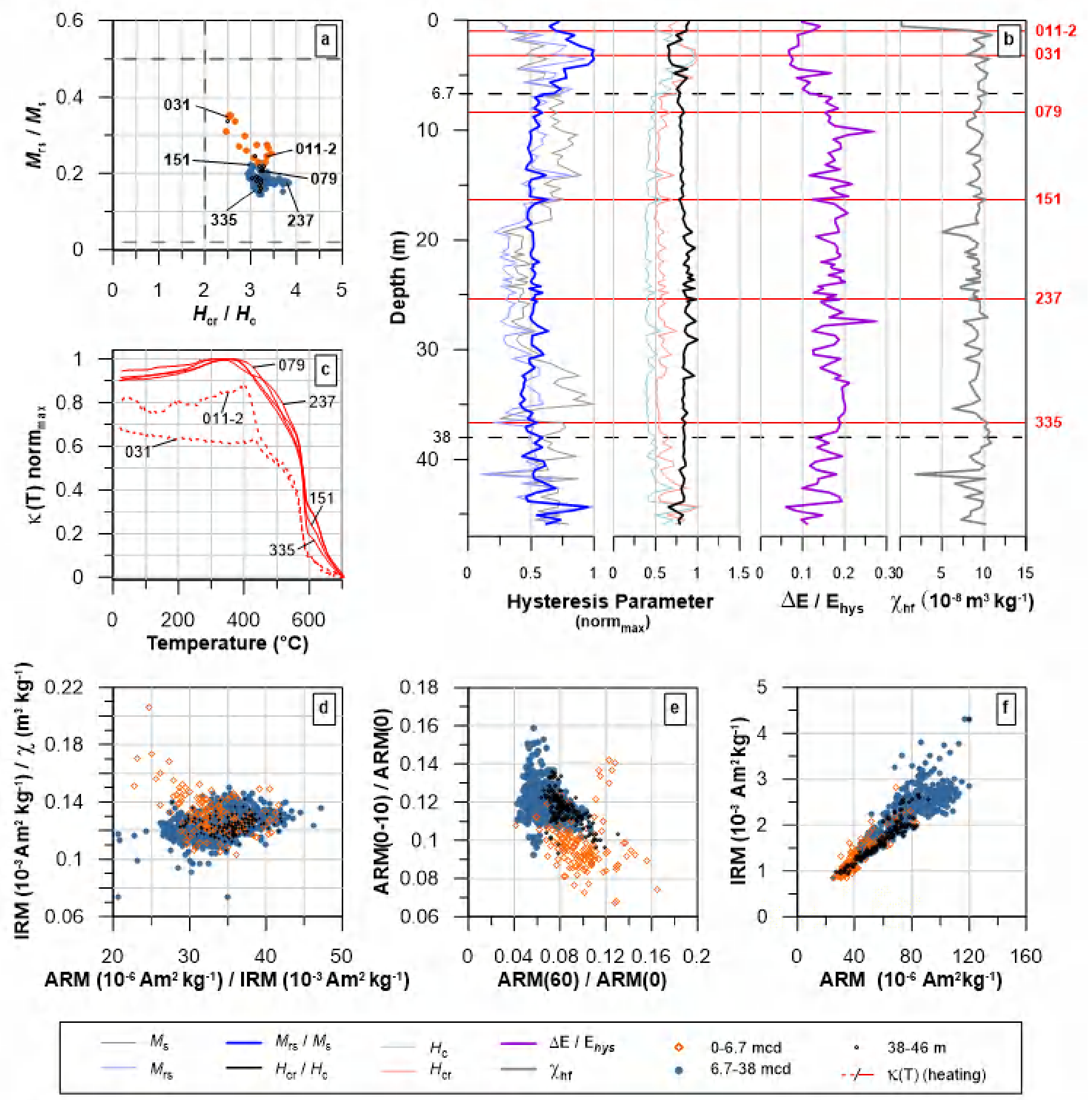

Fig2. Biplots and downcore graphs visualizing mineral magnetic properties using VSM (a,b), Kappabridge (c), and cryogenic magnetometer (d-f) data. (a) hysteresis parameters in the Day plot. (b) downcore variations. M_s, M_{rs}, M_{rs}/M_s, H_c, H_{cr}, and H_{cr}/H_c normalized to the respective maximum. $\Delta E/E_{hys}$ and χ_{hf} in absolute numbers. (c) Heating curves of κ(T). (d) Biplot of grain-size indicators. (e) Plot of ARM fraction remaining after 60 mT demagnetization versus ARM fraction demagnetized below 10 mT. (d) IRM versus ARM.

13. 白垩纪至中新世西北太平洋板块的动力学约束：Mineoka 蛇绿岩的古地磁和 Ar-Ar 年龄

翻译人：李海 12031330@mail.sustech.edu.cn

Ganbat, A, Pastor-Galán, D, Hirano, N, et al. ***Cretaceous to Miocene NW Pacific Plate kinematic constraints: Paleomagnetism and Ar-Ar geochronology in the Mineoka Ophiolite Mélange (Japan)[J].*** *Journal of Geophysical Research: Solid Earth,2021, 126, e2020JB021492. https://doi.org/10.1029/2020JB021492*

摘要: Mineoka 蛇绿岩位于于太平洋，菲律宾海，欧亚大陆和北美板块的交汇处。其成因具有争议，被认为是一个完全俯冲的板块或太平洋和菲律宾板块的一部分。本文基于新的古地磁数据和玄武岩的 40Ar/39Ar 年龄，重建 Mineoka 蛇绿岩与太平洋板块的关系。在对古纬度进行标准分析的基础上，对席状粗粒岩脉进行了净构造旋转分析，以推断蛇绿岩的古扩张方向。分析表明，85-80 Ma，MOR 枕状玄武岩在 16°N 喷发，50 Ma 左右，在 34°N 形成。净构造旋转分析表明，展布方向为 NE 60°。MORBs 的 Ar-Ar 年龄为 53-49 Ma，岛弧玄武岩为 41-35 Ma。该蛇绿岩的形成发生在北太平洋 Nemuro-Olyutorsky 弧的弧后扩张时期。由此推测，Izanagi 的消亡引发了俯冲跃升并导致极性倒转。俯冲开始于平行于山脊的方向，在菲律宾海床向北运动期间，一块原始的后弧地壳被困在日本海沟附近。太平洋板块和菲律宾海板块之间的运动产生了一个高度不稳定的环境，留下了一个被俯冲带包围的小型板块(“Mineoka”)。

ABSTRACT: The Mineoka Ophiolite Mélange is located at the intersection of the Pacific, Philippine Sea, Eurasian, and North American plates. The Mineoka ophiolite origin is disputed, and it has been ascribed to a fully subducted plate or part of the Pacific and Philippine Sea plates. In this paper, we present a kinematic reconstruction of the Mineoka Ophiolite Mélange and its relation with the Pacific Plate, based on new paleomagnetic data and bulk-rock 40Ar/39Ar ages of basaltic rocks. In addition to standard analyses for paleolatitudes, we performed a Net tectonic rotation analysis on

sheeted dolerite dikes to infer the paleospreading direction that formed the ophiolite. The analysis shows that 85-80 Ma MOR pillow basalts erupted at a paleolatitude of N ~16˚, whereas ~50 Ma basalts formed at N ~34˚. Net Tectonic Rotation analysis suggests that the spreading direction was NE 60˚. Ar-Ar ages yielded 53-49 Ma for MORBs and 41-35 Ma for island - arc basalts. The formation of this ophiolite occurred in the back - arc spreading of the Nemuro - Olyutorsky arcs of the NW Pacific. It infers that the final consumption of Izanagi below Japan instigated a subduction jump and flipped its polarity. Subduction initiated parallel to the ridge, and a piece of the original back - arc crust got trapped near the Japan trench during the northwards motion of the Philippine Sea Plate. The contrasting motion between the Pacific and the Philippine Sea plates generated a highly unstable setting followed by a subduction zone that left a small - sized and short - lived plate ("Mineoka"), surrounded by subduction zones.

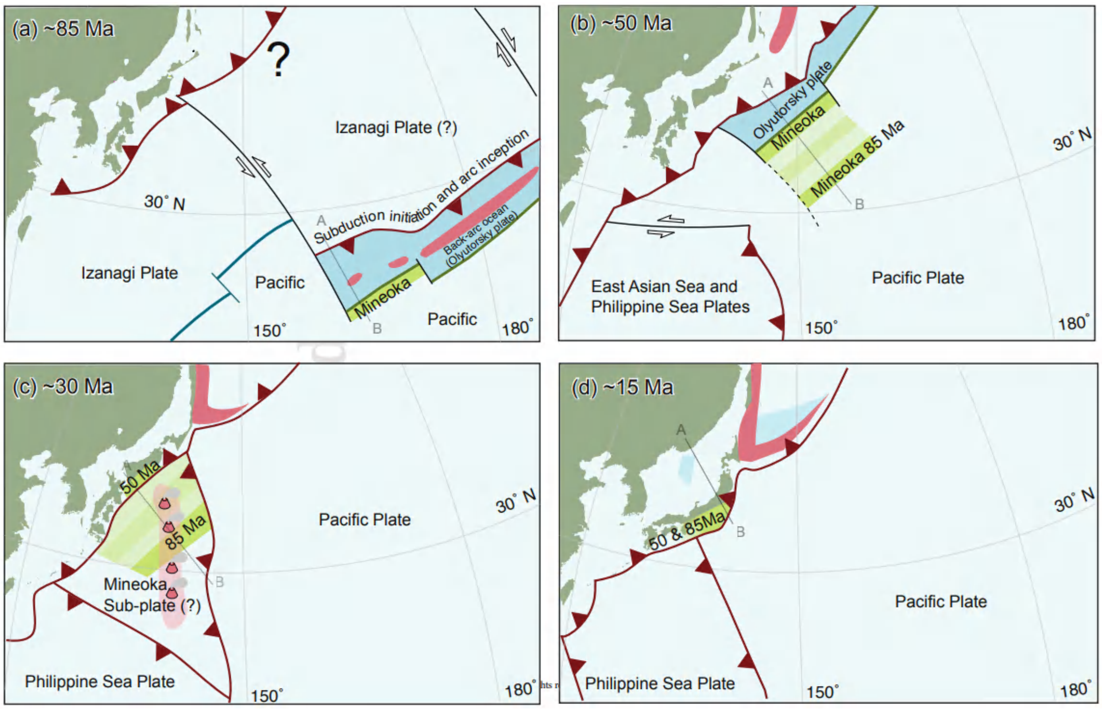

Fig1. Snapshots of the proposed plate - kinematic reconstruction of the Mineoka ophiolite at NW Pacific region at ca. (a) ~85 Ma, (b) ~50 Ma, (c) ~30 Ma, and (d) ~15 Ma. The red lines represent the reconstructed location of the subduction and triangles are subducting directions. Green lines indicate the Olyutorsky-Pacific plate boundary and its putative isochron, which has originated as a

back-arc after the subduction initiation at ~85 Ma. The blue line marks the mid-ocean ridge between Izanagi and Pacific plates. Pink polygons show Nemuro–Olyutorsky arc, light blue polygons outline newly formed oceanic basins, and solid blue polygon marks Olyutorsky plate. The reconstruction follows the mantle reference frame of Doubrovine et al. (2012).